

1 **Functional partnership between carbonic anhydrase and malic enzyme in promoting**
2 **gluconeogenesis in *Leishmania major***

3 Dipon Kumar Mondal^{¶1}, Dhiman Sankar Pal^{¶1,2}, Mazharul Abbasi^{1,3} and Rupak Datta^{*1}

4 ¹Department of Biological Sciences, Indian Institute of Science Education and Research
5 (IISER) Kolkata, Mohanpur, West Bengal, INDIA

6

7 *To whom correspondence to be addressed

8 Rupak Datta

9 E-mail: rupakdatta@iiserkol.ac.in

10 Tel: +91 033 6634 0000; Extn: 1214

11

12 ORCID identifier: Dipon Kumar Mondal: 0000-0002-1065-971X; Dhiman Sankar Pal: 0000-
13 0002-8442-3507; Mazharul Abbasi: 0000-0002-3124-4548; Rupak Datta: 0000-0003-1820-
14 9251

15

16 [¶]These authors contributed equally to this work

17 ²Present Address: Department of Cell Biology and Center for Cell Dynamics, School of
18 Medicine, Johns Hopkins University, Baltimore, MD 21205, USA.

19 ³Present Address: Department of Microbiology, Narayangarh Government College, Rathipur,
20 Narayangarh, West Bengal 721437, India.

21

22 **Running title:** Carbonic anhydrase and malic enzyme partnership in gluconeogenesis

23 **Abbreviations:** CA, carbonic anhydrase; ME, malic enzyme; PC, pyruvate carboxylase;
24 PPDK, pyruvate phosphate dikinase; PEPCK, phosphoenolpyruvate carboxykinase; FBP,
25 fructose-1,6-bisphosphatase

26 **Abstract**

27 *Leishmania* has a remarkable ability to proliferate under widely fluctuating levels of essential
28 nutrients, such as glucose. For this the parasite is heavily dependent on its gluconeogenic
29 machinery. One perplexing aspect of gluconeogenesis in *Leishmania* is the lack of the crucial
30 pyruvate carboxylase (PC) gene. PC-catalyzed conversion of pyruvate to oxaloacetate is a
31 key entry point through which gluconeogenic amino acids are funnelled into this pathway.
32 Absence of PC in *Leishmania* thus raises question about the mechanism of pyruvate entry
33 into the gluconeogenic route. We report here that this task is accomplished in *Leishmania*
34 *major* through a novel functional partnership between its mitochondrial malic enzyme
35 (LmME) and cytosolic carbonic anhydrase (LmCA1). Using a combination of
36 pharmacological inhibition studies with genetic manipulation, we showed that both these
37 enzymes are necessary in promoting gluconeogenesis and supporting parasite growth under
38 glucose limiting condition. Functional crosstalk between LmME and LmCA1 was evident
39 when it was observed that the growth retardation caused by inhibition of any one of these
40 enzymes could be protected to a significant extent by overexpressing the other enzyme. We
41 also found that while LmCA1 exhibited constitutive expression, LmME protein level was
42 strongly upregulated in low glucose condition. Notably, both LmME and LmCA1 were found
43 to be important for survival of *Leishmania* amastigotes within host macrophages. Taken
44 together, our results indicate that LmCA1 by virtue of its CO₂ concentrating ability stimulates
45 LmME-catalyzed pyruvate carboxylation, thereby driving gluconeogenesis through pyruvate-
46 malate-oxaloacetate bypass pathway. Additionally, our study establishes LmCA1 and LmME
47 as promising therapeutic targets.

48

49 **Key words:** Carbonic anhydrase, malic enzyme, gluconeogenesis, pyruvate carboxylation,
50 *Leishmania*

51 **Introduction**

52 *Leishmania* spp. belongs to the trypanosomatid group of protozoan parasites. They are the
53 causative agents of Leishmaniasis, a poverty-associated neglected tropical disease prevalent
54 in almost 100 countries around the world. With about 12 million affected individuals, an
55 estimated 1 million new cases and 20,000-30,000 deaths every year, leishmaniasis continues
56 to be a global public health problem [1–3]. Depending on the species of *Leishmania* involved,
57 the disease is manifested by a broad range of symptoms that ranges from disfiguring skin
58 lesions to life-threatening infection of the internal organs like liver and spleen [3]. Since
59 *Leishmania* vaccine is still not available, management of the disease solely relies on the
60 limited number of anti-leishmanial drugs. However, wide spread emergence of drug resistant
61 strains, drug-induced toxicity and high cost of treatment highlights the urgency for extensive
62 investigation of unexplored metabolic pathways of the parasite with an eye for novel drug
63 targets [4–7].

64 One of the fascinating properties of *Leishmania* is its digenetic life cycle, alternating between
65 sand fly vector and mammalian host. During this process, the flagellated promastigote forms
66 of *Leishmania*, that colonizes sand fly midgut, are injected into mammalian host through
67 proboscis. Following this, the parasites are phagocytosed by macrophages, either directly or
68 via apoptotic neutrophils, and are then transformed to non-flagellated amastigotes within the
69 acidic phagolysosomes [8,9]. How *Leishmania* can survive and proliferate in such diverse
70 physiological niche of varying pH and nutrient availability is a fundamental question that has
71 intrigued researchers over the years [10–12]. Metabolic adaptation to fluctuating
72 carbohydrate levels in its surroundings is once such challenging task accomplished by
73 *Leishmania* [11,13].

74 Hart *et. al.* reported that glucose uptake and utilization in *Leishmania mexicana*
75 promastigotes is several folds higher than in the amastigotes [14]. This is possibly due to the

76 fact that under physiological condition, *Leishmania* promastigotes can easily access glucose
77 from carbohydrate-rich milieu of sand fly midgut [15]. Glucose availability for *Leishmania*
78 amastigotes residing within the phagolysosomal compartment is reported to be much more
79 restricted. Rather, lysosome being the primary site for protein/macromolecular degradation,
80 the environment is rich amino acids and amino sugars [12,16,17]. This change in nutritional
81 environment leads to extensive metabolic reprogramming in the amastigotes that is reflected
82 by significant lowering of glucose transport rate and switch to gluconeogenic mode of energy
83 metabolism whereby intracellular parasites synthesize carbohydrates from non-carbohydrate
84 precursors [11,13]. Although the pathway of gluconeogenesis and its regulation is extensively
85 studied in mammalian system, much less is known about it in lower eukaryotes, particularly
86 in *Leishmania*.

87 Indispensable role of gluconeogenesis in determining *Leishmania* virulence was first reported
88 by Naderer *et. al.* [18]. By creating a *Leishmania major* null mutant strain of an important
89 gluconeogenic enzyme, fructose-1,6-bisphosphatase (FBP), they showed that the Δfbp mutant
90 amastigotes were unable to grow in cultured macrophage cells or in mice. Interestingly, Δfbp
91 *L. major* promastigotes, which grew normally in glucose rich medium, were not able to grow
92 at all in glucose depleted medium. The wild type promastigotes could, however, grow in
93 absence of glucose, albeit slowly. Thus, it was evident that gluconeogenesis is also functional
94 in *Leishmania* promastigotes and they may utilize this machinery during occasional period of
95 glucose starvation [18]. Such situation may arise in the sand fly midgut in between two sugar
96 rich meals [15]. Following this initial discovery, glycerol kinase (GK), phosphoenolpyruvate
97 carboxykinase (PEPCK) and pyruvate phosphate dikinase (PPDK) were identified as key
98 players of gluconeogenesis in *L. Mexicana* [19]. Among these enzymes, PEPCK was shown
99 to be upregulated in response to glucose starvation in *Leishmania donovani*, suggesting that

100 the parasite can sense glucose level in its surroundings and accordingly modulate its
101 gluconeogenic activity [20].

102 Despite these progresses, there are several gaps in our understanding regarding the precise
103 mechanism of gluconeogenesis in *Leishmania*. The mode of pyruvate entry into the
104 gluconeogenic cycle is one such grey area. During prolonged period of glucose starvation in
105 higher eukaryotes, gluconeogenic amino acids, such as alanine, cysteine, glycine, serine,
106 threonine, are first catabolised to pyruvate in the cytosol. Pyruvate is then transported to the
107 mitochondrial matrix with the help of a mitochondrial pyruvate carrier, following which it is
108 converted to oxaloacetate by the enzyme pyruvate carboxylase (PC) [21,22]. This bicarbonate
109 (HCO_3^-)- requiring carboxylation reaction is a critical step through which the central
110 metabolite pyruvate is channelled into the gluconeogenic pathway [23]. Source of this HCO_3^-
111 required for pyruvate carboxylation remained elusive for years. Dodgson *et. al.* provided an
112 important clue by demonstrating that treatment of hepatocytes with carbonic anhydrase (CA)
113 inhibitor, ethoxzolamide, resulted in inhibition of pyruvate carboxylation as well as glucose
114 synthesis in a dose dependent manner [24]. These findings provided the first hint that the
115 mitochondrial carbonic anhydrase V (CAV), by virtue of its CO_2 hydration activity, might be
116 supplying the crucial HCO_3^- substrate for the PC-catalyzed reaction [24,25]. Unambiguous
117 evidence supporting the functional involvement of mitochondrial CA in gluconeogenesis was
118 provided by Shah *et. al.* by detailed characterization of the CAVA and CAVB knockout mice
119 [26]. Despite these mechanistic insights from the mammalian system (Fig. 1A), how pyruvate
120 carboxylation happens in *Leishmania* is still poorly understood.

121 We recently identified two CAs in *L. major* (LmCA1 and LmCA2) and reported their
122 combined role in maintaining cytosolic pH homeostasis in the parasite [27,28]. Whether they
123 play any other physiological role in *Leishmania*, especially in facilitating the process of
124 pyruvate carboxylation during gluconeogenesis has not been explored so far. In this report,

125 we provide strong evidence to demonstrate that the cytosolic CA isoforms in *L. major*
126 (LmCA1) is functionally involved in promoting gluconeogenesis and in supporting parasite
127 growth under glucose limiting condition. However, exact role of LmCA1 in gluconeogenesis
128 was difficult to explain because of the absence of a bona fide PC gene in the genome of all
129 *Leishmania* species [29,30]. Also, PC activity could not be detected in *L. mexicana*
130 promastigotes as well as in amastigotes [31]. This led us to the question, does LmCA1
131 facilitates pyruvate carboxylation via an alternate mechanism? Apart from PC, pyruvate
132 carboxylating activity of malic enzyme (ME), in catalyzing conversion of pyruvate to malate,
133 has been previously reported in few cases in mammalian cells as well as in *Arabidopsis*
134 *thaliana* [32–36]. Furthermore, presence of a functionally active ME from *L. major*
135 (henceforth referred to as LmME) has recently been identified. Although the kinetic
136 parameters of this enzyme have been determined, its role in *Leishmania* physiology is yet to
137 be deciphered [37]. We were thus provoked to hypothesize that LmCA1 might be
138 functionally cooperating with LmME in facilitating pyruvate carboxylation and in driving
139 gluconeogenesis through pyruvate - malate - oxaloacetate bypass pathway. We tested this
140 hypothesis by a combination of pharmacological inhibition and genetic overexpression
141 studies and showed for the first time that this enzyme indeed has a pyruvate carboxylating
142 activity and plays an important role in gluconeogenesis in cooperation with LmCA1. We
143 further demonstrated that LmME is localized in the mitochondria and its expression is
144 upregulated under glucose limiting condition. Finally, by performing macrophage infection
145 experiments it was proven that both LmME as well as LmCA1 are required for intracellular
146 survival of *Leishmania*. Collectively, these results resolved an important paradox with respect
147 to pyruvate carboxylation in *Leishmania* thus helped in better understanding of its
148 gluconeogenic pathway.

149 **Results**

150 **Treatment with CA inhibitor caused *L. major* growth inhibition under glucose-limiting**
151 **condition due to reduced gluconeogenesis and ATP production**

152 Prior studies have implicated role of mammalian CAV, localized in mitochondria, in
153 synthesizing glucose from pyruvate. It was suggested that CAV promotes gluconeogenesis by
154 facilitating the bicarbonate-dependent carboxylation reaction catalyzed by pyruvate
155 carboxylase (Fig. 1A) [24–26]. Although genome of all *Leishmania* species lack evidence for
156 the presence of a bona fide pyruvate carboxylase gene, we were curious to check if one of the
157 LmCAs may still participate in the gluconeogenic process [28,29]. For this, we grew *L. major*
158 promastigotes in absence or presence of increasing concentrations of zineb, which was
159 recently identified as a potent inhibitor of CA activity in *L. major* [27]. Interestingly, zineb
160 caused a dose-dependent inhibition of parasite growth when they were cultured in low glucose
161 medium (0.6mM glucose) in presence of several gluconeogenic amino acids. But this
162 treatment had a minimal effect when 5.6mM exogenous glucose was added to the growth
163 medium (Fig. 1B, C). These results suggested that CA activity might be crucial for
164 *Leishmania* to synthesize glucose from non-carbohydrate precursors. Involvement of LmCA
165 in gluconeogenesis was further supported by the observation that zineb-mediated inhibition
166 of parasite growth in glucose-limiting condition could be completely prevented by
167 supplementing the growth media with 5mM oxaloacetate, an intermediate of the
168 gluconeogenesis pathway (Fig. 1A, D). To validate this result, we engineered a *L. major*
169 strain overexpressing PEPCK (LmPEPCK:OE), a key upstream enzyme of the gluconeogenic
170 pathway (Fig. S1). Interestingly, LmPEPCK:OE strain was much less susceptible to zineb-
171 mediated growth inhibition ($EC_{50} = 0.590\mu\text{M}$) as compared to the wild type ($EC_{50} =$
172 $0.295\mu\text{M}$), indicating that overexpression of this gluconeogenic enzyme can mitigate the

173 adverse effect of inhibition of LmCA activity. Finally, we measured glucose and ATP levels
174 in *L. major* cells in absence or presence of zineb (Table 1). It was observed that zineb
175 treatment caused ~50% reduction in the glucose and ATP levels in *L. major* cells growing
176 under glucose-limiting condition (0.6mM glucose). Supplementation of the growth media
177 with exogenous glucose or oxaloacetate provided complete protection against zineb-mediated
178 depletion of glucose and ATP levels thereby providing an unambiguous evidence for the
179 involvement of LmCA in gluconeogenesis in *Leishmania* cells.

180 **LmCA1 but not LmCA2 is involved in gluconeogenesis in *L. major***

181 We recently reported that *L. major* expresses a cytosolic and a plasma membrane bound CA
182 and named them as LmCA1 and LmCA2, respectively [28]. So, the obvious question was
183 which of these two LmCAs participate in the gluconeogenesis process? To address this, we
184 utilized the LmCA1^{+/-} and LmCA2^{+/-} heterozygous strains and the corresponding genetic
185 complementation strain of *L. major* that were earlier generated and validated by us [28]. It
186 was observed that in glucose-limiting condition, the LmCA1^{+/-} heterozygous strain grew
187 sluggishly as compared to the wild type strain and exhibited 36% reduction in the total
188 number of cells after 72 hours. The growth rate of the corresponding complementation strain
189 (LmCA1^{+/-}:CM) was near-normal thereby confirming that single allele disruption of LmCA1
190 is indeed responsible for the observed growth defect of the mutant strain in glucose-limiting
191 condition (Fig. 2A). However, the LmCA1^{+/-} strain did not exhibit any growth defect when
192 exogenous glucose was added in the media (Fig. 2B). Exogenous addition of oxaloacetate
193 also could completely restore the growth defect of the LmCA1^{+/-} strain in glucose-limiting
194 condition implying that LmCA1 participates in the gluconeogenesis process (Fig. 2C). It is
195 worth noting that the growth rate of the LmCA2^{+/-} strain was similar to that of its wild type
196 counterpart in glucose-limiting as well as glucose rich conditions (Fig. 2A, B). To further test
197 the contribution of LmCA1 and LmCA2 in *Leishmania* cell growth under glucose-limiting

198 condition, we generated two *L. major* strains overexpressing either LmCA1 or LmCA2
199 (LmCA1:OE, LmCA2:OE) (Fig. S1). The LmCA1:OE, LmCA2:OE and the wild type *L.*
200 *major* cells were grown in glucose-limiting condition and their susceptibilities to the CA
201 inhibitor zineb were compared. Interestingly, as compared to the wild type *L. major*, cells
202 overexpressing LmCA1 was significantly less susceptible to zineb-mediated growth
203 inhibition (EC_{50} values were $0.295\mu\text{M}$ and $0.597\mu\text{M}$ for wild type and LmCA1:OE,
204 respectively). LmCA2 overexpressing strain on the other hand were quite similar to its wild
205 type counterpart in terms of zineb susceptibility (Fig. 2D). Collectively, these data suggest
206 that LmCA1, but not LmCA2, plays an important role in sustaining parasite growth in low
207 sugar environment. Apart from sluggish growth phenotype, the LmCA1^{+/-} strain, in glucose-
208 limiting condition, also exhibited crippled morphology with significant reduction in cell
209 length. This phenotype was reversed to a significant extent in the LmCA1^{+/-}: CM
210 complementation strain (Fig. 2E, F). Our morphological data suggest that single allele
211 disruption of LmCA1 makes the parasite susceptible metabolic stress in low-glucose
212 environment. Metabolic stress in the LmCA1^{+/-} strain under glucose-deprived condition was
213 even more evident when we found that its glucose and ATP contents was significantly less
214 compared to that in wild type *L. major* (more than 40% drop for both glucose and ATP). As
215 expected, glucose and ATP levels in the LmCA1^{+/-}: CM complementation strain was almost
216 same as that in the wild type cells thus confirming that LmCA1 is indeed involved in glucose
217 and ATP synthesis in *L. major*. The LmCA1^{+/-} strain showed no signs of glucose or ATP
218 depletion when exogenous glucose or oxaloacetate was supplemented in the growth medium.
219 It is noteworthy that the LmCA2^{+/-} strain even under glucose-limiting condition had normal
220 glucose and ATP levels (Table 2). Our data thus provide compelling evidence that LmCA1,
221 but not LmCA2, is involved in gluconeogenesis and ATP production in *L. major*.

222 **Functional cooperation between LmCA1 and LmME in promoting gluconeogenesis and**
223 **in sustaining parasite growth under glucose-limiting condition**

224 Although our results provided unambiguous evidence to support the role of LmCA1 in
225 gluconeogenesis, it remains unclear how it participates in the process. It is well established
226 that CAs facilitate various metabolic reactions by providing the crucial HCO_3^- to different
227 carboxylating enzymes [38]. However, absence of the PC gene in *Leishmania* genome raises
228 question about the possible metabolic partner of LmCA1 [29,30]. How oxaloacetate could be
229 synthesized bypassing the pyruvate carboxylase reaction was also a mystery. We were
230 intrigued to come across few prior studies where pyruvate carboxylating activity of ME was
231 reported in heart, skeletal muscle, neuronal cells as well as in plant [33,35,36,39]. This led us
232 to hypothesize that LmCA1 might facilitate bicarbonate-dependent pyruvate carboxylation by
233 a leishmanial ME (Fig. 3A). This notion was strengthened by the fact that a functional ME
234 from *L. major* has recently been identified by Giordana *et. al.* Although kinetic and structural
235 properties of this enzyme (henceforth referred to as LmME) were reported, its physiological
236 function is still unknown [37]. Thus, in order to study the physiological function of this
237 enzyme and its possible role in gluconeogenesis we first looked for a potent pharmacological
238 inhibitor of LmME. A high throughput screening by Ranzani *et. al.* led to identification of
239 several inhibitors against two ME isoforms of *Trypanosoma cruzi* [40]. From this large list of
240 inhibitors, we procured three compounds (ATR4-003, ATR6-001, and ATR7-010) based on
241 their high efficiency in inhibiting the *T. cruzi* MEs and potent trypanocidal activity (Fig. S2)
242 [40]. To test whether these compounds can also act as LmME inhibitors, we first cloned
243 LmME cDNA in pET28a vector, expressed the protein in *E. coli* BL21(DE3) and eventually
244 purified it to homogeneity (Fig. S3, 3B). The purified LmME catalyzed NADP^+ -dependent
245 decarboxylation of malate to pyruvate as well as NADPH -dependent carboxylation of
246 pyruvate to malate as reflected by specific activity data (Fig. 3C). Purification of LmME in

247 active form thus allowed us to test efficacies of the potential inhibitors. We found that
248 although ATR4-003 and ATR6-001 did not inhibit LmME activity up to a concentration of
249 20 μ M (data not shown), ATR7-010 could inhibit malate decarboxylating and pyruvate
250 carboxylating activity of LmME with IC₅₀ values of 1.595 μ M and 1.556 μ M, respectively
251 (Fig. 3D). Encouraged by this finding, we next checked if ATR7-010 treatment could affect
252 *L. major* growth. Data presented in Fig. 3E shows that ATR7-010 treatment caused a dose
253 dependent inhibition of parasite growth in glucose-deprived condition with an EC₅₀ value of
254 13.7 μ M. To check if this stunted growth is indeed due to LmME inhibition, we generated a *L.*
255 *major* strain overexpressing LmME (LmME:OE) (Fig. S1). As expected, LmME:OE strain
256 exhibited significantly less susceptibility to ATR7-010-mediated growth inhibition under
257 glucose-deprived condition (with EC₅₀ value of 24.2 μ M as compared to 13.7 μ M for the wild
258 type). Interestingly, ATR7-010-mediated growth inhibition of the wild type *L. major* could be
259 prevented to a significant extent by exogenous addition of glucose or oxaloacetate (EC₅₀
260 values increased by > 2.5 folds in both the cases). These results gave us the first indication
261 that similar to LmCA1, LmME might also be playing an important role in gluconeogenesis.
262 To investigate whether there is any functional cooperation between LmME and LmCA1 we
263 checked for ATR7-010 susceptibility of the LmCA1 overexpressing *L. major*. Strikingly,
264 LmCA1:OE strain showed almost two folds decrease in susceptibility to the LmME inhibitor,
265 ATR7-010, under glucose-deprived condition (Fig. 3E). To crosscheck the functional
266 cooperation between LmME and LmCA1, we performed the reverse experiment whereby we
267 determined susceptibility of the LmME overexpressing strain to LmCA inhibitor, zineb. We
268 found that indeed LmME overexpression provided significant protection against zineb-
269 mediated growth inhibition under glucose limiting condition (EC₅₀ values were 0.295 μ M and
270 0.722 μ M for wild type and LmME:OE strains, respectively). Taken together, these results

271 indicate that LmCA1 functionally cooperates with LmME to promote gluconeogenesis and
272 *Leishmania* cell growth under glucose limiting environment. Treatment with ATR7-010 not
273 only affected *Leishmania* growth, but also induced significant morphological deformities
274 resulting in dose dependent shortening of cell length (Fig. 3G, H). Such crippled morphology
275 is an indicator of metabolic stress, which became more obvious when we measured
276 intracellular glucose and ATP levels in the ATR7-010 treated parasites. Data presented in
277 Table 3 shows that there was >30% drop in intracellular glucose and ATP levels in the
278 ATR7-010 treated *L. major* cells as compared to their untreated counterpart. Exogenous
279 supplementation with glucose or oxaloacetate completely protected against depletion of these
280 key metabolites thereby providing strong evidence supporting the involvement of LmME in
281 gluconeogenesis. It is worth noting that intracellular glucose and ATP contents were
282 significantly more in the LmME:OE strain compared to that in the wild type *L. major*. This
283 data suggests that efficiency of gluconeogenesis in the parasite can be controlled by tweaking
284 LmME expression.

285 **LmME expression and activity is regulated by glucose**

286 Following the lead from our finding that genetic overexpression LmME could result in
287 increased production of glucose and ATP, we next explored whether LmME expression can
288 be regulated under physiological context. Glucose has been widely reported to be a
289 physiological regulator of gene expression in many cell types in which glucose signalling
290 pathways serves as a fundamental mechanism to optimize different metabolic activities [41–
291 43]. In fact, glucose starvation was shown to upregulate the gluconeogenic enzyme PEPCK
292 in *L. donovani* [20]. This led us to check if LmME expression is regulated by glucose. From
293 our RTqPCR results it is clear that the LmME transcript levels remained unaltered
294 irrespective of the amount of glucose present in the growth medium (Fig. 4A). To analyze
295 LmME expression at the protein level we first generated a rabbit polyclonal antibody

296 against the protein (Fig. S4A). We used this antibody to analyze LmME protein levels in *L.*
297 *major* promastigotes growing in glucose-limiting (low glucose) or glucose-supplemented
298 (high glucose) medium by western blot. In contrast to our RTqPCR data, we observed that
299 LmME protein level was significantly upregulated (more than two folds) in the parasites
300 growing under low glucose condition than those in high glucose (Fig. 4B). The status of
301 LmME was independently verified by immunofluorescence staining, the result of which are
302 in agreement with the western blot data (Fig. 4C). It is worth noting that varying glucose
303 concentration in growth medium did not alter LmCA1 expression either at mRNA or at
304 protein level as determined by RTqPCR and western blot analysis using anti-LmCA1
305 antibody (Fig. S4B, S5). We next compared LmME activities in whole cell lysate of parasites
306 growing in glucose-limiting or glucose-supplemented medium. We observed that although
307 malate decarboxylating activity remained unaltered, there was ~ 20% increase in pyruvate
308 carboxylating activity of LmME in *Leishmania* cells growing in glucose-limiting condition as
309 opposed to those having access to exogenously added glucose. An even more striking
310 observation was that while malate decarboxylating activity was ~1.5 folds more than the
311 pyruvate carboxylating activity in the purified LmME, the enzyme functioned quite
312 differently when its specific activity was measured in the whole cell lysate. We found that
313 pyruvate carboxylating activity of LmME in *L. major* whole cell lysate is ~5 folds more than
314 the malate decarboxylating activity (Fig. 3C, 4F). Taken together our data suggest that
315 intracellular LmME, especially under low glucose condition, promotes gluconeogenesis by
316 increased protein expression and by selectively augmenting its pyruvate carboxylase activity.

317 **LmME is localized in the mitochondria**

318 As it is evident from our data that there is a functional cooperation between LmCA1 and
319 LmME in triggering gluconeogenesis, precise knowledge about subcellular localization of
320 these two proteins is of utmost importance. We have previously reported LmCA1 to be a

321 cytosolic enzyme, however, localization of LmME is yet to be determined [28]. To predict
322 subcellular localization of LmME we analyzed its sequence using various bioinformatics
323 tools. The reports predicted LmME to be a mitochondrial protein devoid of any
324 transmembrane domain (Table S1). To experimentally determine its subcellular localization,
325 we first developed *L. major* stable transfectants expressing C-terminal GFP-tagged LmME
326 and stained these cells with mitochondria specific marker, Mito Tracker red (Fig. S6).
327 Extensive co-localization of GFP puncta with the Mito Tracker stained vesicles was
328 observed, suggesting mitochondrial localization of LmME (Fig. 5A). While this initial result
329 was promising, we developed an anti-LmME antibody in the meantime and decided to use it
330 to validate localization of the endogenous LmME in wild type *L. major* by biochemical
331 methods. For this, we lysed the cells with digitonin and separated the whole cell lysate into
332 mitochondrial and cytoplasmic fractions. Western blot of the cell fractions with anti-LmME
333 antibody revealed that LmME is exclusively localized in the mitochondrial fraction.
334 Authenticities of the cell fractionations were confirmed by western blots with antibodies
335 against previously reported mitochondrial (LmAPX) and cytosolic (LmCA1) proteins of *L.*
336 *major* (Fig. 5B, S4B) [28,44]. Although our data provided unambiguous evidence in support
337 of mitochondrial localization of LmME, its submitochondrial localization (matrix/membrane)
338 could not be ascertained experimentally due to unavailability of appropriate *Leishmania*
339 specific antibody markers. However, since LmME1 lacks any transmembrane domain, it is
340 likely to be localized in the mitochondrial matrix (Table S1).

341 **LmCA1 and LmME are both crucial for survival of *L. major* within host macrophages**

342 After having proven that LmCA1 cooperates with LmME in sustaining *in vitro* growth of the
343 parasites under glucose limiting condition, we wanted to check the importance of these two
344 enzymes for intracellular propagation of *L. major*. For this, wild type *L. major* were first
345 grown under glucose limiting condition, following which we infected J774A.1 macrophages

346 with these parasites in absence or presence of 0.625 μ M zineb or 25 μ MATR7-010. It was
347 found that in presence of LmCA1 inhibitor (zineb) and LmME inhibitor (ATR7-010) there
348 was 43% and 35% drop in the intracellular parasite burden, respectively as compared to
349 untreated control (Table 4). Based on our previous report and the data presented in Fig. S7, it
350 is worth pointing out that the concentration of inhibitors used in this experiment (0.625 μ M
351 for zineb and 25 μ M for ATR7-010) do not have any effect on macrophage growth [27]. Next,
352 J774A.1 macrophages were infected with the corresponding overexpressing strains of *L.*
353 *major* (LmCA1:OE and LmME:OE). In contrast to the results obtained with the enzyme
354 inhibitors, we observed ~55% spike in intracellular parasite burden for both the strains as
355 compared to their wild type counterpart (Table 4). Taken together, our data confirmed that
356 LmCA1 as well as LmME are indeed very critical for intracellular propagation of *L. major*.
357 Interestingly, in all these experimental conditions there was not much difference in the
358 percentage of infected macrophages, which varied from 86 – 96%, suggesting that LmCA1
359 and LmME possibly do not play any major role in infectivity of the parasite (Table 4).

360 **Discussion**

361 Ability to synthesize glucose from non-carbohydrate precursors via gluconeogenesis is the
362 mainstay for survival of several organisms under sugar limiting condition [45]. This
363 metabolic pathway is particularly important for the *Leishmania* parasites, which grows within
364 the amino acid rich phagolysosomal compartment [12,17,46]. Although some of the
365 gluconeogenic enzymes of *Leishmania* were earlier identified through elegant studies, very
366 little is known about the details of the entire pathway [18,19]. Absence of the PC encoding
367 gene in *Leishmania* genome was especially perplexing and hence the mechanism of pyruvate
368 entry into the gluconeogenic circuit remained elusive till date [29]. Our work revealed that
369 LmME, by virtue of its unconventional pyruvate carboxylating activity, drives
370 gluconeogenesis in *L. major* with help of the CO₂ concentrating enzyme, LmCA1. This

371 unique functional partnership between cytosolic LmCA1 and mitochondrial LmME was
372 found to be critical for growth of *Leishmania* promastigotes when glucose availability was
373 restricted. Both of these enzymes also played determining roles in establishing intracellular
374 *Leishmania* infection within host macrophages. Thus, apart from providing new mechanistic
375 insights into the gluconeogenic pathway of *Leishmania*, our results highlights LmCA1 and
376 LmME as prospective drug targets, worthy of further exploration.

377 The first step of gluconeogenesis in mammals involves conversion of pyruvate to
378 oxaloacetate by the mitochondrial enzyme PC. This is a critical entry point through which
379 several gluconeogenic amino acids are funnelled into the *de novo* glucose synthesis pathway
380 [22,45]. PC is a biotin-dependent carboxylase that uses HCO_3^- as the donor of the carboxyl
381 group [22]. Mitochondrial CAV is known to facilitate the PC-catalyzed carboxylation
382 reaction by providing this crucial HCO_3^- [24,26]. Although CAV is a well-established player
383 of mammalian gluconeogenesis, there is no information regarding gluconeogenic capability
384 of CAs in lower vertebrates, invertebrates or in microorganisms [38]. In this context, our data
385 showing the role of LmCA1 in supporting gluconeogenesis in *L. major* is possibly the first
386 evidence of gluconeogenic activity of a CA in lower eukaryotes. This exciting result was,
387 however, difficult to comprehend because *Leishmania* genome does not encode a *bona fide*
388 PC gene [29,30]. How LmCA1 participates in the gluconeogenesis process in absence of its
389 metabolic partner PC was an intriguing question for us.

390 It was earlier proposed that in absence of PC, the parasite may utilize the enzyme pyruvate
391 phosphate dikinase (PPDK) to directly synthesize phosphoenolpyruvate (PEP) from pyruvate
392 without having to go through the oxaloacetate intermediate [19]. But experiments with
393 ΔPPDK mutant *Leishmania* confirmed that PPDK do not play any role in gluconeogenesis in
394 *Leishmania* promastigotes. Although PPDK was shown to be responsible for pyruvate entry
395 into the gluconeogenic pathway in axenic amastigotes, functional importance of this enzyme

396 is yet to be established in intracellular amastigotes [19]. Thus, it is evident that the available
397 information on PPK function in *Leishmania* fails to provide a comprehensive understanding
398 of the PC-independent mechanism of pyruvate entry into the gluconeogenic pathway. Neither
399 does it clarify the exact role of LmCA1 in this process. These ambiguities were finally
400 removed with the identification of LmME as an important player of the gluconeogenesis in *L.*
401 *major*. Our data suggests that pyruvate carboxylating activity of LmME provides an
402 alternative mode of pyruvate entry into the gluconeogenic pathway via pyruvate – malate –
403 oxaloacetate route. This is supported by the observation that pyruvate-carboxylation was the
404 dominant activity of LmME in *L. major* whole cell lysate. This is in stark contrast to the
405 purified enzyme, in which the malate-decarboxylating activity was found to be dominant.
406 This interesting data suggests that some unknown factors in *Leishmania* cells may act as
407 LmME regulator in promoting its pyruvate carboxylating activity *in vivo*.

408 ME is a ubiquitous enzyme that catalyzes reversible decarboxylation of malate in presence
409 NADP to produce pyruvate, CO₂ and NADPH [47]. Although the enzyme exhibits both
410 carboxylating and decarboxylating activity when assayed *in vitro*, malate-decarboxylation
411 was shown to be responsible for most of the reported physiological function of ME. The
412 reducing equivalent (NADPH), generated as a byproduct of this decarboxylation reaction,
413 was shown to promote fatty acid biosynthesis and maintain redox balance in various
414 organisms [48–52]. Relatively much less is known regarding the physiological role of the
415 pyruvate-carboxylating activity of ME. Hassel B *et. al.* reported that ME-catalyzed pyruvate
416 carboxylation in rat neurons results in synthesis of TCA cycle intermediates that in turn
417 promotes production of the neurotransmitter glutamate [33]. Apart from this, pyruvate-
418 carboxylating activity of ME was shown to play a role in anaplerosis in hypertrophied heart
419 as well as in plant (*Arabidopsis thaliana*) whereby malate produced in the cytosol is
420 transported to mitochondria for fuelling the TCA cycle [35,36]. Our finding showing

421 participation of LmME in gluconeogenesis in *Leishmania* through its pyruvate-carboxylating
422 activity thus uncovers a novel physiological function of ME.

423 Functional partnership between LmME and LmCA1 is another interesting revelation of this
424 study. That the adverse effect of LmCA1 inhibition on *L. major* cell growth under glucose
425 limiting condition could be prevented to a significant extent by overexpression of LmME
426 (and vice versa) is a testimony of the fact that these two enzymes indeed cooperates with each
427 other. CAs are known to play a crucial role in metabolism by providing the CO₂/bicarbonate
428 to various carbon fixing enzymes (e.g. PC, carbamoyl phosphate synthetase, RuBisCO) that
429 incorporates CO₂ to the corresponding substrates [38,53]. Our data suggests that LmCA1
430 facilitates the carboxylation reaction catalyzed by LmME in a similar way. We have
431 previously reported that the cytosolic LmCA1 is instrumental in HCO₃⁻ buffering of
432 *Leishmania* cytosol by converting the incoming H⁺ ions into H₂O and CO₂ (). CO₂ being a
433 freely diffusible gas can easily disperse across the mitochondrial membranes having high
434 CO₂-permeability and stimulate pyruvate carboxylating activity of LmME in the lumen of the
435 mitochondria to generate malate [54,55]. This appears to be rational mechanism since ME
436 has a substrate preference for CO₂ as opposed to its counterpart PC, which utilizes HCO₃⁻
437 [22,56,57]. Absence of a mitochondrial CA in *L. major* also seems to be a key factor in
438 maintaining a high luminal concentration of CO₂, which otherwise would have been readily
439 converted to HCO₃⁻. A similar CO₂ concentrating mechanism has been reported in the
440 chloroplast of green-alga. It was shown that a CA present in the thylakoid lumen converts
441 bicarbonate to CO₂, which then diffuses out of the thylakoid double membrane and drives the
442 RuBisCO-catalyzed carboxylation reaction in the stroma [58]. Presence of functionally active
443 malate dehydrogenase (MDH) isoforms in *Leishmania* indicates that the parasite would be
444 able to synthesize oxaloacetate from malate, once the latter is formed by pyruvate
445 carboxylation [59]. Since many of the downstream gluconeogenic enzymes in *Leishmania*

446 and other trypanosomatids (e.g. PEPCK, FBP etc.) are localized in the glycosome, it is likely
447 that the malate formed in the mitochondria is transported to the glycosome before it is
448 converted to oxaloacetate by the catalytically active glycosomal MDH [18,59,60]. The
449 putative malate transporters encoded in the *Leishmania* genome may play an important role
450 in this process by facilitating mitochondria-glycosome malate shuttling [29,30]. A tentative
451 model describing these initial steps of gluconeogenesis in *Leishmania* is outlined in Fig. 6.
452 In addition to their functional role in *L. major* promastigotes, LmCA1 and LmME were also
453 found to be important for intracellular survival of the amastigotes. *Leishmania* amastigotes
454 resides within the phagolysosomal compartment where glucose availability is limited and
455 amino acids are in abundance [12]. LmCA1-LmME metabolic partnership in promoting *de*
456 *novo* synthesis of glucose would thus provide a life support for the parasite residing in such a
457 stringent nutritional environment. Apart from their gluconeogenic role, it is also possible that
458 LmCA1 and LmME might have some other physiological function, which can as well
459 contribute to overall fitness of the amastigotes in withstanding the harsh phagolysosomal
460 conditions. In fact, role of LmCA1 in maintaining cytosolic pH homeostasis and acid
461 tolerance of the parasite is already reported by us [28]. Although a non-gluconeogenic-role
462 for LmME has not been reported yet, this possibility cannot be ruled out completely. In this
463 connection it is worth mentioning that while LmME protein level was induced in low glucose
464 concentration, LmCA1 was constitutively expressed. Since glucose responsive expression is a
465 typical characteristic of many gluconeogenic enzymes, it might be speculated that LmME
466 plays a dedicated role in gluconeogenesis whereas function of LmCA1 is more versatile
467 [20,61–63].
468 To summarize, the metabolic partnership between LmCA1 and LmME reported here reveals a
469 novel bypass pathway in gluconeogenesis that allows PC-independent entry of pyruvate into
470 the gluconeogenic circuit in *Leishmania*. Whether this pathway is operational in any other

471 organism remains to be seen. However, it may be noted that both *Trypanosoma brucei* and
472 *Trypanosoma cruzi* lacks the PC gene in their genome and they both express functional CA
473 and ME [29,30,64]. Thus, the CA-ME bypass route may be a characteristic feature of
474 gluconeogenesis for the entire trypanosomatid family. While this will require experimental
475 validation, our current study has clearly established the functional importance of LmCA1 and
476 LmME and uncovered their potential as antileishmanial drug targets.

477 **Materials and methods**

478 Unless otherwise mentioned, all reagents were purchased from Sigma-Aldrich (St. Louis
479 MO). All primers were bought from Integrated DNA technologies and their sequence details
480 are provided in Table S2.

481 **Preparation of *Leishmania* culture medium containing high or low glucose** 482 **concentration**

483 For our study, glucose-free RPMI 1640 (HiMedia) was used, which is rich in gluconeogenic
484 amino acids. It was supplemented with 15% foetal bovine serum (Gibco), 23.5mM HEPES,
485 0.2mM adenine, 150 µg/ml folic acid, 10 µg/ml hemin, 120 U/ml penicillin, 120 µg/ml
486 streptomycin, and 60 µg/ml gentamicin. This medium was supplemented with or without 5.6
487 mM glucose, and henceforth been referred to as ‘high glucose’ or ‘low glucose’ medium,
488 respectively. pH was adjusted to 7.2 for both media. Total glucose concentration in high or
489 low glucose culture medium was estimated by glucose oxidase-peroxidase assay, as described
490 later in this section. The glucose concentration for high or low glucose culture medium, was
491 found to be 6.2 mM or 0.6 mM, respectively. Glucose in low glucose medium is contributed
492 by foetal bovine serum.

493 **Cell culture and cell growth analysis**

494 Wild type *L. major* promastigotes (strain 5ASKH; generously provided by Dr Subrata Adak
495 of IICB, Kolkata, India) were grown at 26°C, as described by us previously [27,28]. J774A.1

496 (murine macrophage cell line from the National Centre for Cell Science, Pune, India) cells
497 were cultured as described earlier [27,28]. For cell growth analysis, wild type or mutant *L.*
498 *major* cells were seeded in high (6.2 mM) or low (0.6 mM) glucose medium, and their
499 growth was monitored at different time points till 72 hrs by counting the number of cells in
500 haemocytometer. Wherever mentioned, cells grown in low glucose medium were
501 supplemented with 5 mM oxaloacetate (OAA) or 5.6 mM of glucose (Glu). Selection
502 antibiotics were removed from culture medium during the course of all these experiments.
503 CA inhibitor, zineb [zinc ethylene-bis-dithiocarbamate], or ME inhibitors, ATR4-003
504 [Pyrimidin-7-one], ATR6-001 [Tetrahydrothieno- isoquinoline] or ATR7-010 [Triazolo-
505 thiadiazole] (ChemBridge Corporation, San Diego, CA), were used for growth inhibition
506 study [40]. The inhibitors were freshly dissolved in dimethyl sulfoxide (DMSO) to prepare
507 5mM (for zineb) or 100 mM (for ME inhibitors) stock solutions. According to experimental
508 requirements, further dilutions were made in DMSO before addition to the culture medium.
509 *L. major* promastigotes or J774A.1 macrophage were grown in medium containing the
510 inhibitors at desired concentrations for 72 h, following which the cells were analysed using a
511 haemocytometer. Cells incubated with an equivalent concentration of DMSO (0.2%) always
512 acted as untreated controls. The percentage of cell growth was calculated using the formula
513 $(\text{Cell number}_{\text{treated}}/\text{Cell number}_{\text{untreated}} \times 100)$. The growth of the untreated cells was considered
514 as 100%. Finally, 50% effective concentration (EC_{50}) for each inhibitor was calculated from
515 the percentage of cell growth values using OriginPro 8 software. Selection antibiotics were
516 removed from culture medium during the course of all these experiments.

517 **Transfection**

518 Transfection of DNA into *L. major* cells was performed using electroporation as described by
519 us previously [28]. Briefly, 3.6×10^7 log phase wild type or mutant *L. major* promastigotes
520 were incubated with 10-30 μg of the DNA construct in electroporation buffer (21 mM

521 HEPES, 6 mM glucose, 137 mM NaCl and 0.7 mM NaH₂PO₄; pH 7.4) in a 0.2 cm
522 electroporation cuvette for 10 minutes on ice. Subsequently, electroporation was done in a
523 Bio-Rad Gene Pulsar apparatus using 450 volts and 550 µF capacitance. Transfected cells
524 were selected in appropriate antibiotic-containing medium.

525 **Generation of *L. major* strain overexpressing LmPEPCK, LmCA1, LmCA2 or LmME**

526 Primers P1/P2, P3/P4, P5/P6 or P19/P20 (listed in Table S2) were used to PCR-amplify the
527 ORF of LmPEPCK, LmCA1, LmCA2 or LmME gene from genomic DNA of wild type *L.*
528 *major* cells. Amplified LmPEPCK, LmCA1, LmCA2 or LmME gene fragment was cloned
529 into the BamHI/EcoRV sites of pXG-GFP+, SmaI site of pXG-SAT, BamHI site of pXG-
530 PHLEO or BamHI/EcoRV sites of pXG-GFP+ plasmid, respectively, to generate the
531 overexpression (OE) constructs. The clones were subsequently verified by sequencing. 30 µg
532 LmPEPCK:OE, LmCA1:OE, LmCA2:OE or LmME:OE construct was transfected into wild
533 type *L. major* promastigotes by electroporation. Each transfected strain was selected and
534 maintained in 100 µg/ml G418 sulphate, 200 µg/ml nourseothricin (Jena Bioscience), or
535 8 µg/ml phleomycin (Invivogen).

536 **Generation of *L. major* strain expressing GFP-tagged LmME**

537 Primers P7/P8 (listed in Table S2) were used to PCR-amplify the ORF of LmME gene from
538 genomic DNA of wild type *L. major* promastigotes. Amplified gene segment of LmME was
539 cloned into the BamHI and EcoRV sites of pXG-GFP+ vector to generate the C-terminal
540 GFP-tagged construct. The clone was subsequently verified by sequencing. 30 µg LmME-
541 GFP construct was transfected into wild type *L. major* promastigotes by electroporation. The
542 transfected strain was selected and maintained in 100 µg/ml G418 sulphate.

543 **Cloning, bacterial expression and purification of LmME**

544 The ORF of LmME gene was PCR-amplified from wildtype *L. major* genomic DNA using
545 the primer set P9/P10. A 1722 bp amplified gene fragment was cloned within EcoRI/HindIII

546 sites of pET28a+ vector to generate the N-terminal 6xHis-tagged construct. The clone was
547 verified by sequencing. For the purpose of protein expression, this construct was transformed
548 into *E. coli* BL21(DE3) cells. Transformed cells were grown overnight in 5ml LB medium
549 containing 50 µg/ml kanamycin at 37°C. Overnight grown culture was inoculated in 250 ml
550 LB medium. When the culture reached an OD₆₀₀ ~0.6, LmME protein expression was
551 induced in presence of 0.5 mM isopropyl β-D-thiogalactoside (IPTG) for 8 hrs at 20°C.
552 Bacterial cells were harvested, resuspended in ice-chilled lysis buffer (50 mM Tris, 100mM
553 NaCl, 10mM imidazole, 1mg/ml lysozyme and 1mM PMSF; pH 8.0) and incubated on ice for
554 40 min with intermittent vortexing. Cells were lysed using a 10 sec pulse sonicator with 20
555 sec rest on ice. The cell lysate was subsequently centrifuged at 18000 x g for 30 min at 4°C.
556 The cell free supernatant was loaded on to pre-equilibrated Ni²⁺-nitrilotriacetic resin
557 (Qiagen), and incubated for 1hr at 4°C. The resin was washed with wash buffer (50 mM Tris,
558 100mM NaCl, 20mM imidazole and 1mM PMSF; pH 8.0), followed by another wash with
559 the same buffer containing 40 mM imidazole. Finally, 6xHis-tagged LmME protein bound to
560 Ni²⁺-nitrilotriacetic resin was eluted in wash buffer containing 250 mM imidazole. Eluted
561 LmME was dialyzed thrice in dialysis buffer (50 mM Tris, 100mM NaCl and 1mM PMSF; pH
562 8.0). Purity of LmME protein was verified on 10% SDS-PAGE followed by coomassie blue
563 staining.

564 **LmME and LmCA1 antibody generation**

565 Polyclonal antiserum against LmCA1 or LmME was generated by BioBharati Life Science
566 Pvt. Ltd. (custom antibody generation facility), India. Purified LmME protein (dissolved in
567 sterile PBS, pH 7.4), was used for generating antibody as per company protocol. Briefly, 500
568 µg of purified LmME was mixed thoroughly with Freund's Complete Adjuvant (1:1 ratio),
569 and was injected subcutaneously into two adult New Zealand rabbits in equal amounts. After
570 2 weeks, a booster dose of 150 µg purified protein, mixed with Incomplete Freund's

571 Adjuvant, was injected into each rabbit. After 5 such booster doses, 10 ml blood was taken
572 from the ear vein of each rabbit, sera were collected and tested by western blotting on
573 purified LmME (0.5 $\mu\text{g}/\text{well}$) and wild type *Leishmania* whole cell lysate (80 $\mu\text{g}/\text{well}$)
574 samples.

575 The PCR-amplified ORF of LmCA1 gene (primers P11/P12 are listed in Table S2) was
576 cloned within EcoRI site of pET28a+ vector, and the verified N-terminal 6xHis-tagged
577 construct was provided to BioBharati Life Science Pvt. Ltd for LmCA1 antiserum generation.
578 LmCA1 protein was induced in BL21(DE3) *E. coli* cells using 0.5 mM IPTG for 4 hrs at
579 37°C. LmCA1 in the insoluble fraction was used for antigen preparation and administered
580 into adult New Zealand rabbits, as described above. Anti-LmCA1 antiserum was collected
581 and verified by western blotting on LmCA1 (9.25 $\mu\text{g}/\text{well}$) purified to homogeneity from
582 LmCA1-overexpressing *L. major* promastigotes, and wild type *Leishmania* whole cell lysate
583 (120 $\mu\text{g}/\text{well}$) samples.

584 **LmME activity assay**

585 Malic enzyme activity in purified LmME or *L. major* whole cell lysate was assayed on
586 Hitachi U2900 spectrophotometer using quartz cuvette of 1 cm path length as described
587 previously, with minor modifications [32]. To test malate decarboxylation or pyruvate
588 carboxylation activity, the assay mixture was made up of 1 ml malate buffer (50 mM Tris-Cl;
589 pH 7.5, 10 mM malate, 1 mM MnCl_2 and 0.15 mM NADP^+) or pyruvate buffer (50 mM Tris-
590 Cl buffer; pH 5.5, 1 mM MnCl_2 , 0.15 mM NADPH, 50 mM pyruvate and 75 mM NaHCO_3),
591 respectively. After incubating in the spectrophotometer at 37°C for 5 min to achieve
592 temperature equilibrium, malate decarboxylation or pyruvate carboxylation reaction was
593 initiated with the addition of 5 μg purified enzyme or 100 μg whole cell lysate. Absorbance
594 was recorded at 340 nm from 0-2min. The average malate decarboxylation or pyruvate
595 carboxylation activity from three different protein preparations or promastigote cultures was

596 expressed in enzyme units (EU)/mg, where 1 unit of enzymatic activity is defined as the
597 amount of enzyme that catalyses production or consumption of 1 μ mol of NADPH per
598 minute, respectively. Enzyme activity was calculated by considering molar extinction
599 coefficient for NADPH is 6.22 mM⁻¹cm⁻¹. The total protein concentration of the purified
600 enzyme or whole cell lysate was measured by the method of Lowry *et al* [65]. For inhibition
601 studies, the inhibitors (at desired concentrations) were incubated with purified LmME for 5
602 mins at room temperature prior to the assay. The 50% enzyme activity inhibitory
603 concentration (IC₅₀) for each inhibitor was calculated in triplicate using Origin Pro8.0
604 program.

605 **Imaging studies**

606 Morphology of *L. major* promastigotes was determined by Zeiss Supra 55VP scanning
607 electron microscope (SEM) as described by us previously [27,28]. At least 50 cells were
608 analysed for each experimental condition using ImageJ software. During the course of the
609 experiment, selection antibiotics were removed from culture medium.

610 To determine subcellular localization of LmME in *L. major*, LmME-GFP expressing cells
611 were mounted on poly L-lysine coated coverslips for 1 hr. Attached parasites were then
612 stained with 500 nM MitotrackerRed CMX-Ros (Invitrogen) in the dark for 30 mins [66].
613 Post-incubation, cells were washed in PBS to remove excess stain, air-dried, and finally
614 embedded in anti-fade mounting medium containing DAPI (VectaShield from Vector
615 Laboratories). Images were acquired with a Zeiss LSM 710 confocal microscope. During the
616 course of the experiment, selection antibiotics were removed from culture medium.

617 For investigating LmME expression in *L. major*, wild type cells were grown in low (0.6 mM)
618 or high (6.2 mM) glucose medium for 48 hrs. Subsequently, cells were mounted on poly L-
619 lysine coated coverslips, fixed with methanol: acetone (1:1), and permeabilized with 0.1%
620 triton X-100. 0.2% gelatine was used to block non-specific binding. Next, cells were

621 incubated with anti-LmME primary antibody (1:1500) for 1.5 hrs. Cells were washed with
622 PBS and incubated with a secondary goat anti-rabbit Alexa Fluor 488 antibody (1:600;
623 Molecular Probes) for 1.5 hrs in the dark. Post-incubation, cells were washed with PBS and
624 embedded in anti-fade mounting medium containing DAPI. Images were acquired with a
625 Zeiss LSM 710 confocal microscope. Mean fluorescence intensity for different samples was
626 quantified using MacBiophotonics ImageJ software. At least 50 cells were analysed for each
627 set of experiment.

628 **Subcellular fractionation and western blot analysis**

629 Cytoplasmic and mitochondrial fractions were isolated from wild type *L. major* whole cell
630 lysates as described previously [67,68]. Briefly, 1×10^8 promastigotes were harvested and
631 washed in MES buffer (20mM MOPS, pH 7.0, 250mM sucrose, 3mM EDTA). Cells were
632 resuspended in 0.2 ml MES buffer containing 1 mg/ml digitonin and protease inhibitor
633 cocktail, and incubated at RT for 10 min. The resultant whole cell lysate was centrifuged
634 at $10,000 \times g$ for 5 min. The supernatant was collected as the cytoplasmic fraction whereas the
635 pellet was dissolved in MES buffer and used as the mitochondrial fraction.

636 SDS-PAGE (10%) was performed with the subcellular fractions (sample loaded was
637 equivalent to 5×10^6 cells). LmME was detected with rabbit anti-LmME antisera (1:4000). The
638 authenticity of the cytoplasmic or mitochondrial fraction was verified by western blotting
639 using rabbit anti-*L. major* carbonic anhydrase or -LmCA1 (1:1000) or rabbit anti-*L. major*
640 ascorbate peroxidase or -LmAPX (1:50, a generous gift from Dr Subrata Adak, IICB, India)
641 [44]. After overnight primary antibody incubation at 4°C, blots were probed with anti-rabbit
642 horseradish peroxidase (HRP)-conjugated secondary antibody (1:4000; Thermo Scientific)
643 for 2 hrs. SuperSignal West Pico Chemiluminescent substrate (Thermo Scientific) was used
644 to develop the blots, and chemiluminescent signal was detected in the ChemiDoc imaging
645 system (Syngene).

646 To investigate relative expression of LmME (63.4 kDa) or LmCA1 (35.4 kDa) in wild type *L.*
647 *major*, 1×10^8 cells were grown in high (6.2 mM) or low (0.6 mM) glucose medium,
648 harvested, resuspended in 200 μ l 1X PBS (containing 1 mM PMSF) and lysed by sonication.
649 SDS-PAGE (10%) was performed with samples obtained from 5×10^6 cells. LmME or
650 LmCA1 was detected with rabbit anti-LmME or -LmCA1 antiserum, as described earlier.
651 Expression of β -actin, detected by rabbit anti-*L. donovani* β -actin antibody (1:4000; a
652 generous gift by Dr Amogh Sahasrabudhe, CSIR-CDRI) and anti-rabbit HRP-conjugated
653 secondary antibody (1:4000), was considered as the endogenous control [69]. Densitometry
654 value of LmME protein bands was quantified using MacBiophotonics ImageJ software.
655 To check LmME purified in bacterial expression system, 10 μ g of purified protein was
656 loaded on 10% SDS-PAGE and detected by western blotting using primary anti-His antibody
657 (1:2000; Bio Bharati Life Science Pvt. Ltd.), followed by anti-rabbit HRP-conjugated
658 secondary antibody (1:4000).

659 **Measurement of glucose concentration**

660 Intracellular glucose in *L. major* promastigotes was measured by an end-point colorimetric
661 assay, involving the sequential catalytic actions of glucose oxidase (GOD) and peroxidase
662 (POD) enzymes, as described previously with minor modifications [70,71]. 2.5×10^8 *L. major*
663 cells, grown in low (0.6 mM) glucose medium, were harvested, resuspended in PBS and
664 lysed by sonication. Subsequently, glucose assay solution (98% GOD-POD reagent and 2%
665 o-dianisidine) was added to whole cell lysate and the entire mixture was incubated for 30
666 mins at 37°C. After incubation, the reaction was stopped by adding 12 N H₂SO₄, which also
667 allowed formation of a stable coloured product. Finally, the absorbance of samples was
668 measured against the reagent blank at 540 nm. The glucose concentration for each sample
669 was obtained from the corresponding absorbance value using a calibration curve. The
670 calibration curve was generated by recording absorbance as a function of glucose

671 concentration by checking the absorbance of increasing concentrations of glucose (0.625-
672 20 μ M). Selection antibiotics were removed from culture medium during the course of the
673 experiment. Glucose concentration in the *L. major* culture medium was also measured using
674 this method.

675 **Determination of intracellular ATP content**

676 Intracellular ATP level in *L. major* promastigotes was measured using firefly luciferase and
677 its substrate D-luciferin, as described previously [72]. Briefly, 4×10^7 *L. major* cells, grown in
678 low (0.6 mM) glucose medium, were harvested, resuspended in 50 μ l of 1X PBS and lysed
679 by sonication. 10 μ l whole cell lysate was added to ATP standard reaction solution which
680 was freshly prepared as per manufacturer's instructions. After incubation for 15 mins at room
681 temperature, luminescence of the sample was measured at 560 nm. ATP concentration for
682 each sample was obtained from the corresponding luminescence value using a calibration
683 curve. The calibration curve was generated by recording luminescence as a function of ATP
684 concentration by measuring the luminescence of increasing concentrations of ATP (75–
685 600nM). Selection antibiotics were removed from culture medium during the entire course of
686 the experiment.

687 **Quantification of RNA transcript in *Leishmania***

688 1×10^8 wild type or mutant *L. major* promastigotes were harvested and total RNA was
689 extracted using TRIzol reagent. Subsequently, DNase I treatment was performed to remove
690 DNA contamination, as per the manufacturer's instruction. 1 μ g of total RNA was used to
691 synthesize cDNA with the help an oligo(dT) primer and Moloney murine leukaemia virus
692 reverse transcriptase (RT). Expression of LmPEPCK (1578 bp), LmCA1 (921 bp), LmCA2
693 (1887 bp) or LmME (1722 bp) transcript in wild type or mutant *L. major* was checked by
694 semi-quantitative RT-PCR using gene-specific primers P1/P2, P3/P4, P5/P6 or P9/P10
695 respectively (listed in Table S2). The number of cycles was optimized at 28 after examination

696 of the yield of PCR products at a range of 24–30 cycles. Relative expression of LmPEPCK,
697 LmCA1, LmCA2 or LmME mRNA was normalized using wild type cells as reference sample
698 and rRNA45 gene as an endogenous control. rRNA45 amplification (143 bp) from cDNA
699 was done using primers P13/P14 (listed in Table S2). Relative expression of LmME or
700 LmCA1 gene in wild type cells, grown in high (6.2 mM) or low (0.6 mM) glucose medium,
701 was measured by Real time PCR using primers P15/P16 or P17/P18 (Table S2). Real-time
702 PCR was done on the Step One Real-Time PCR system (Applied Biosystems) using SYBR
703 Green PCR Master Mix. Relative expression level of LmME or LmCA1 mRNA was
704 normalized with wild type cells grown in high glucose medium as a reference sample and
705 rRNA45 gene as the endogenous control using a Comparative C_T method as mentioned by the
706 manufacturer.

707 **Quantification of intracellular parasite load**

708 Infection of J774A.1 murine macrophages with *L. major* was performed as described by us
709 previously [27,28]. Briefly, macrophages were activated with *E. coli* lipopolysaccharide (100
710 ng/ml) for 6 hrs. Activated macrophages were infected with stationary phase cultures of wild
711 type or overexpressing *L. major* strains, grown in low (0.6 mM) glucose medium, at a
712 parasite to macrophage ratio of 30:1 for 12 hrs. Post-infection, all non-phagocytosed parasites
713 were removed with PBS, and the infected macrophages were incubated for 18 hrs. During
714 this period, wild type *L. major*-infected macrophages were incubated in absence or presence
715 of 25 μ M ATR7-010 or 0.625 μ M zineb. Subsequently cells were washed with PBS, fixed with
716 acetone: methanol (1:1) and embedded in anti-fade mounting medium with DAPI. Parasite
717 load (number of amastigotes per 100 macrophages) for each strain/treatment was quantified
718 by counting the total number of DAPI-stained nuclei of macrophages and amastigotes in a
719 field, using an epifluorescence microscope (IX81, Olympus). For each condition, at least 100
720 macrophages (and corresponding number of amastigotes) were analysed. The percentage of

721 macrophages infected by wild type (untreated or inhibitor-treated) or overexpressing *L. major*
722 strains was determined by counting the total number of DAPI-stained nuclei of uninfected
723 and infected macrophages in a field. For each condition, at least 100 macrophages were
724 analysed.

725 **Bioinformatic analysis of LmME**

726 LmME (LmjF24.0770) cDNA and protein sequences were obtained from *L. major* gene
727 database [29,30]. Subcellular localization for LmME was predicted by analysing its primary
728 sequence using the online prediction software, TargetP v1.1 to predict presence of any of the
729 N-terminal signal sequence for targeting a protein to ER, mitochondria or chloroplast,
730 TMHMM v2.0 to predict transmembrane helices, BaCelLo to predict presence of a nuclear
731 localization signal, and PTS1 predictor to predict peroxisome targeting signal 1 [73–76].

732 **Statistical analysis**

733 All statistical analyses were calculated by paired or Student's t test using GraphPad software.
734 All results were expressed as the mean \pm SD from at least 3 independent experiments. P-
735 values indicating statistical significance were grouped into values of ≤ 0.05 and < 0.001 ; *
736 $p \leq 0.05$, ** $p < 0.01$, *** $p < 0.001$.

737 **Author contributions**

738 DKM, DSP, MA performed the experiments, DKM, DSP analyzed the data and wrote the
739 initial draft of the manuscript, RD conceived and supervised the work, analyzed all data and
740 wrote the final manuscript.

741 **Acknowledgements**

742 The authors sincerely thank Mr. Ritabrata Ghosh, Mr. Susnata Karmakar, Mr. Kashinath
743 Sahu, and Mr. Sujoy Bose for their technical assistance. The authors are thankful to Drs.
744 Jayasri Das Sarma, Mohit Prasad, and Supratim Datta of IISER Kolkata and Drs. Subrata
745 Adak and Dr. Amogh Sahasrabudhe of CSIR-IICB and CSIR-CDRI, respectively for their

746 help with various reagents used in this work. The authors also thank Drs. Sankar Maiti and
747 Piyali Mukherjee of IISER Kolkata and Presidency University, respectively, for helpful
748 discussion and constructive suggestions. This research was supported by the Department of
749 Biotechnology (DBT) and Department of Science and Technology (DST) grants
750 BT/PR21170/MED/29/1109/2016 and EMR/2017/004506, respectively. DKM. and DSP
751 were supported by IISER Kolkata fellowships, MA was supported by University Grants
752 Commission fellowship.

753 **Competing interests**

754 The authors declare no competing or financial interests.

755 **References**

- 756 1 Alvar J, Vélez ID, Bern C, Herrero M, Desjeux P, Cano J, Jannin J & de Boer M (2012)
757 Leishmaniasis worldwide and global estimates of its incidence. *PLoS One* **7**.
- 758 2 Okwor I & Uzonna J (2016) Social and Economic Burden of Human Leishmaniasis. *Am J*
759 *Trop Med Hyg* **94**, 489–493.
- 760 3 Burza S, Croft SL & Boelaert M (2018) Leishmaniasis. *Lancet* **392**, 951–970.
- 761 4 Croft SL, Sundar S & Fairlamb AH (2006) Drug resistance in leishmaniasis. *Clin Microbiol*
762 *Rev* **19**, 111–126.
- 763 5 Sundar S, Chakravarty J, Rai VK, Agrawal N, Singh SP, Chauhan V & Murray HW (2007)
764 Amphotericin B Treatment for Indian Visceral Leishmaniasis: Response to 15 Daily
765 versus Alternate-Day Infusions. *Clin Infect Dis* **45**, 556–561.
- 766 6 Sundar S & Olliaro PL (2007) Miltefosine in the treatment of leishmaniasis: Clinical
767 evidence for informed clinical risk management. *Ther Clin Risk Manag* **3**, 733–740.
- 768 7 Sundar S & Jaya J (2010) Liposomal amphotericin B and leishmaniasis: Dose and response.
769 *J Glob Infect Dis* **2**, 159.
- 770 8 Chang K-P & Dwyer DM (1978) Leishmania Donovanii. Hamster macrophage interactions

- 771 in vitro: cell entry, intracellular survival, and multiplication of amastigotes. *J Exp Med*
772 **147**, 515–530.
- 773 9 Peters NC, Egen JG, Secundino N, Debrabant A, Kimblin N, Kamhawi S, Lawyer P, Fay
774 MP, Germain RN & Sacks D (2008) In vivo imaging reveals an essential role for
775 neutrophils in leishmaniasis transmitted by sand flies. *Science (80-)* **321**, 970–974.
- 776 10 Burchmore RJS & Barrett MP (2001) Life in vacuoles - Nutrient acquisition by
777 *Leishmania* amastigotes. *Int J Parasitol* **31**, 1311–1320.
- 778 11 McConville MJ & Naderer T (2011) Metabolic Pathways Required for the Intracellular
779 Survival of *Leishmania*. *Annu Rev Microbiol* **65**, 543–561.
- 780 12 McConville MJ, de Souza D, Saunders E, Likic VA & Naderer T (2007) Living in a
781 phagolysosome; metabolism of *Leishmania* amastigotes. *Trends Parasitol* **23**, 368–375.
- 782 13 Saunders EC, Ng WW, Kloehn J, Chambers JM, Ng M & McConville MJ (2014)
783 Induction of a Stringent Metabolic Response in Intracellular Stages of *Leishmania*
784 mexicana Leads to Increased Dependence on Mitochondrial Metabolism. *PLoS Pathog*
785 **10**.
- 786 14 Hart DT & Coombs GH (1982) *Leishmania mexicana*: Energy metabolism of amastigotes
787 and promastigotes. *Exp Parasitol* **54**, 397–409.
- 788 15 Abbasi I, Trancoso Lopo de Queiroz A, Kirstein OD, Nasereddin A, Horwitz BZ, Hailu A,
789 Salah I, Mota TF, Fraga DBM, Veras PST, Poche D, Poche R, Yeszhanov A, Brodskyn
790 C, Torres-Poche Z & Warburg A (2018) Plant-feeding phlebotomine sand flies, vectors
791 of leishmaniasis, prefer *Cannabis sativa*. *Proc Natl Acad Sci U S A* **115**, 11790–11795.
- 792 16 Naderer T, Heng J & McConville MJ (2010) Evidence that intracellular stages of
793 *Leishmania major* utilize amino sugars as a major carbon source. *PLoS Pathog* **6**.
- 794 17 McConville MJ, Saunders EC, Kloehn J & Dagley MJ (2015) *Leishmania* carbon
795 metabolism in the macrophage phagolysosome- feast or famine? *FI000Research* **4**, 938.

- 796 18 Naderer T, Ellis MA, Sernee MF, De Souza DP, Curtis J, Handman E & McConville MJ
797 (2006) Virulence of *Leishmania major* in macrophages and mice requires the
798 gluconeogenic enzyme fructose-1,6-bisphosphatase. *Proc Natl Acad Sci U S A* **103**,
799 5502–5507.
- 800 19 Rodriguez-Contreras D & Hamilton N (2014) Gluconeogenesis in *Leishmania mexicana*:
801 Contribution of glycerol kinase, phosphoenolpyruvate carboxykinase, and pyruvate
802 phosphate dikinase. *J Biol Chem* **289**, 32989–33000.
- 803 20 Saini S, Kumar Ghosh A, Singh R, Das S, Abhishek K, Kumar A, Verma S, Mandal A,
804 Hasan Sardar A, Purkait B, Kumar A, Kumar Sinha K & Das P (2016) Glucose
805 deprivation induced upregulation of phosphoenolpyruvate carboxykinase modulates
806 virulence in *Leishmania donovani*. *Mol Microbiol* **102**, 1020–1042.
- 807 21 McCommis KS & Finck BN (2015) Mitochondrial pyruvate transport: A historical
808 perspective and future research directions. *Biochem J* **466**, 443–454.
- 809 22 Jitrapakdee S, St Maurice M, Rayment I, Cleland WW, Wallace JC & Attwood P V.
810 (2008) Structure, mechanism and regulation of pyruvate carboxylase. *Biochem J* **413**,
811 369–387.
- 812 23 Menefee AL & Zeczycki TN (2014) Nearly 50 years in the making: Defining the catalytic
813 mechanism of the multifunctional enzyme, pyruvate carboxylase. *FEBS J* **281**, 1333–
814 1354.
- 815 24 Dodgson SJ (1987) Inhibition of mitochondrial carbonic anhydrase and ureagenesis: A
816 discrepancy examined. *J Appl Physiol* **63**, 2134–2141.
- 817 25 Hazen SA, Waheed A, Sly WS, Lanoue KF & Lynch CJ (1996) Differentiation-dependent
818 expression of CA V and the role of carbonic anhydrase isozymes in pyruvate
819 carboxylation in adipocytes. *FASEB J* **10**, 481–490.
- 820 26 Shah GN, Rubbelke TS, Hendin J, Nguyen H, Waheed A, Shoemaker JD & Sly WS

- 821 (2013) Targeted mutagenesis of mitochondrial carbonic anhydrases VA and VB
822 implicates both enzymes in ammonia detoxification and glucose metabolism. *Proc Natl*
823 *Acad Sci U S A* **110**, 7423–7428.
- 824 27 Pal DS, Mondal DK & Datta R (2015) Identification of metal dithiocarbamates as a novel
825 class of antileishmanial agents. *Antimicrob Agents Chemother* **59**, 2144–2152.
- 826 28 Pal DS, Abbasi M, Mondal DK, Varghese BA, Paul R, Singh S & Datta R (2017)
827 Interplay between a cytosolic and a cell surface carbonic anhydrase in pH homeostasis
828 and acid tolerance of Leishmania. *J Cell Sci* **130**, 754–766.
- 829 29 Logan-Klumpler FJ, De Silva N, Boehme U, Rogers MB, Velarde G, McQuillan JA,
830 Carver T, Aslett M, Olsen C, Subramanian S, Phan I, Farris C, Mitra S, Ramasamy G,
831 Wang H, Tivey A, Jackson A, Houston R, Parkhill J, Holden M, Harb OS, Brunk BP,
832 Myler PJ, Roos D, Carrington M, Smith DF, Hertz-Fowler C & Berriman M (2012)
833 GeneDB-an annotation database for pathogens. *Nucleic Acids Res* **40**.
- 834 30 Aslett M, Aurrecochea C, Berriman M, Brestelli J, Brunk BP, Carrington M, Depledge
835 DP, Fischer S, Gajria B, Gao X, Gardner MJ, Gingle A, Grant G, Harb OS, Heiges M,
836 Hertz-Fowler C, Houston R, Innamorato F, Iodice J, Kissinger JC, Kraemer E, Li W,
837 Logan FJ, Miller JA, Mitra S, Myler PJ, Nayak V, Pennington C, Phan I, Pinney DF,
838 Ramasamy G, Rogers MB, Roos DS, Ross C, Sivam D, Smith DF, Srinivasamoorthy G,
839 Stoeckert CJ, Subramanian S, Thibodeau R, Tivey A, Treatman C, Velarde G & Wang
840 H TriTrypDB: a functional genomic resource for the Trypanosomatidae. .
- 841 31 Mottram JC & Coombs GH (1985) Leishmania mexicana: Enzyme activities of
842 amastigotes and promastigotes and their inhibition by antimonials and arsenicals. *Exp*
843 *Parasitol* **59**, 151–160.
- 844 32 ŻELEWSKI M & ŚWIERCZYŃSKI J (1991) Malic enzyme in human liver: Intracellular
845 distribution, purification and properties of cytosolic isozyme. *Eur J Biochem* **201**, 339–

- 846 345.
- 847 33 Hassel B & Bråthe A (2000) Neuronal pyruvate carboxylation supports formation of
848 transmitter glutamate. *J Neurosci* **20**, 1342–1347.
- 849 34 Heart E, Cline GW, Collis LP, Pongratz RL, Gray JP & Smith PJS (2009) Role for malic
850 enzyme, pyruvate carboxylation, and mitochondrial malate import in glucose-stimulated
851 insulin secretion. *Am J Physiol - Endocrinol Metab* **296**.
- 852 35 Pound KM, Sorokina N, Ballal K, Berkich DA, Fasano M, Lanoue KF, Taegtmeier H,
853 O'donnell JM & Lewandowski ED (2009) Substrate-enzyme competition attenuates
854 upregulated anaplerotic flux through malic enzyme in hypertrophied rat heart and
855 restores triacylglyceride content: Attenuating upregulated anaplerosis in hypertrophy.
856 *Circ Res* **104**, 805–812.
- 857 36 Badia MB, Mans R, Lis A V., Tronconi MA, Arias CL, Maurino VG, Andreo CS,
858 Drincovich MF, van Maris AJA & Gerrard Wheeler MC (2017) Specific Arabidopsis
859 thaliana malic enzyme isoforms can provide anaplerotic pyruvate carboxylation function
860 in *Saccharomyces cerevisiae*. *FEBS J* **284**, 654–665.
- 861 37 Giordana L, Sosa MH, Leroux AE, Mendoza EFR, Petray P & Nowicki C (2018)
862 Molecular and functional characterization of two malic enzymes from *Leishmania*
863 parasites. *Mol Biochem Parasitol* **219**, 67–76.
- 864 38 Henry RP (1996) Multiple Roles of Carbonic Anhydrase in Cellular Transport and
865 Metabolism. *Annu Rev Physiol* **58**, 523–538.
- 866 39 Swierczyński J (1980) Purification and some properties of extramitochondrial malic
867 enzyme from rat skeletal muscle. *Biochim Biophys Acta* **616**, 10–21.
- 868 40 Ranzani AT, Nowicki C, Wilkinson SR & Cordeiro AT (2017) Identification of Specific
869 Inhibitors of *Trypanosoma cruzi* Malic Enzyme Isoforms by Target-Based HTS. *SLAS*
870 *Discov* **22**, 1150–1161.

- 871 41 Meugnier E, Rome S & Vidal H (2007) Regulation of gene expression by glucose. *Curr*
872 *Opin Clin Nutr Metab Care* **10**, 518–522.
- 873 42 Towle HC (2005) Glucose as a regulator of eukaryotic gene transcription. *Trends*
874 *Endocrinol Metab* **16**, 489–494.
- 875 43 Johnston M (1999) Feasting, fasting and fermenting: Glucose sensing in yeast and other
876 cells. *Trends Genet* **15**, 29–33.
- 877 44 Dolai S, Yadav RK, Pal S & Adak S (2008) Leishmania major ascorbate peroxidase
878 overexpression protects cells against reactive oxygen species-mediated cardioplipin
879 oxidation. *Free Radic Biol Med* **45**, 1520–1529.
- 880 45 Hers HG & Hue L (1983) Gluconeogenesis and Related Aspects of Glycolysis. *Annu Rev*
881 *Biochem* **52**, 617–653.
- 882 46 Chang KP & Dwyer DM (1978) Leishmania donovani: Hamster macrophage interactions
883 in vitro: Cell entry, intracellular survival, and multiplication of amastigotes*. *J Exp Med*
884 **147**, 515–530.
- 885 47 Gu-Gang Chang* ‡ and & Tong§ L (2003) Structure and Function of Malic Enzymes, A
886 New Class of Oxidative Decarboxylases†. .
- 887 48 Zhu B-H, Zhang R-H, Lv N-N, Yang G-P, Wang Y-S & Pan K-H (2018) The Role of
888 Malic Enzyme on Promoting Total Lipid and Fatty Acid Production in Phaeodactylum
889 tricornutum. *Front Plant Sci* **9**, 826.
- 890 49 Hao G, Chen H, Wang L, Gu Z, Song Y, Zhang H, Chen W & Chen YQ (2014) Role of
891 malic enzyme during fatty acid synthesis in the oleaginous fungus Mortierella alpina.
892 *Appl Environ Microbiol* **80**, 2672–2678.
- 893 50 Murai S, Ando A, Ebara S, Hirayama M, Satomi Y & Hara T (2017) Inhibition of malic
894 enzyme 1 disrupts cellular metabolism and leads to vulnerability in cancer cells in
895 glucose-restricted conditions. *Oncogenesis* **6**.

- 896 51 Chang YL, Gao HW, Chiang CP, Wang WM, Huang SM, Ku CF, Liu GY & Hung HC
897 (2015) Human mitochondrial NAD(P)⁺-dependent malic enzyme participates in
898 cutaneous melanoma progression and invasion. *J Invest Dermatol* **135**, 807–815.
- 899 52 Allmann S, Morand P, Ebikeme C, Gales L, Biran M, Hubert J, Brennand A, Mazet M,
900 Franconi JM, Michels PAM, Portais JC, Boshart M & Bringaud F (2013) Cytosolic
901 NADPH homeostasis in glucose-starved procyclic trypanosoma brucei relies on malic
902 enzyme and the pentose phosphate pathway fed by gluconeogenic flux. *J Biol Chem*
903 **288**, 18494–18505.
- 904 53 Cannon GC, Heinhorst S & Kerfeld CA (2010) Carboxysomal carbonic anhydrases:
905 Structure and role in microbial CO₂ fixation. *Biochim Biophys Acta - Proteins*
906 *Proteomics* **1804**, 382–392.
- 907 54 Endeward V, Al-Samir S, Itef F & Gros G (2014) How does carbon dioxide permeate cell
908 membranes? A discussion of concepts, results and methods. *Front Physiol* **4 JAN**.
- 909 55 Arias-Hidalgo M, Hegermann J, Tsiavalariis G, Carta F, Supuran CT, Gros G &
910 Endeward V (2016) CO₂ and HCO₃⁻ Permeability of the Rat Liver Mitochondrial
911 Membrane. *Cell Physiol Biochem* **39**, 2014–2024.
- 912 56 Dalziel K & Londesborough JC (1968) The mechanisms of reductive carboxylation
913 reactions. Carbon dioxide or bicarbonate as substrate of nicotinamide-adenine
914 dinucleotide phosphate-linked isocitrate dehydrogenase and malic enzyme. *Biochem J*
915 **110**, 223–230.
- 916 57 HÄSLER RE, HOLTUM JAM & LATZKO E (1987) CO₂ is the inorganic carbon
917 substrate of NADP malic enzymes from *Zea mays* and from wheat germ. *Eur J Biochem*
918 **163**, 619–626.
- 919 58 Raven JA (1997) CO₂-concentrating mechanisms: A direct role for thylakoid lumen
920 acidification? *Plant, Cell Environ* **20**, 147–154.

- 921 59 Leroux A, Fleming-Canepa X, Aranda A, Maugeri D, Cazzulo JJ, Sánchez MA &
922 Nowicki C (2006) Functional characterization and subcellular localization of the three
923 malate dehydrogenase isozymes in *Leishmania* spp. *Mol Biochem Parasitol* **149**, 74–85.
- 924 60 Sommer JM, Nguyen TT & Wang CC (1994) Phosphoenolpyruvate carboxykinase of
925 *Trypanosoma brucei* is targeted to the glycosomes by a C-terminal sequence. *FEBS Lett*
926 **350**, 125–129.
- 927 61 Massillon D, Barzilai N, Chen W, Hu M & Rossetti L (1996) Glucose regulates in vivo
928 glucose-6-phosphatase gene expression in the liver of diabetic rats. *J Biol Chem* **271**,
929 9871–9874.
- 930 62 Decaux J-F, Antoine B & Kahn A (1989) *THE JOURNAL OF BIOLOGICAL*
931 *CHEMISTRY Regulation of the Expression of the L-type Pyruvate Kinase Gene in Adult*
932 *Rat Hepatocytes in Primary Culture**.
- 933 63 Decaux JF, Marcillat O, Pichard AL, Henry J & Kahn A (1991) Glucose-dependent and -
934 independent effect of insulin on gene expression. *J Biol Chem* **266**, 3432–3438.
- 935 64 Opperdoes FR & Cotteem D (1982) Involvement of the glycosome of *trypanosoma brucei*
936 in carbon dioxide fixation. *FEBS Lett* **143**, 60–64.
- 937 65 LOWRY OH, ROSEBROUGH NJ, FARR AL & RANDALL RJ (1951) Protein
938 measurement with the Folin phenol reagent. *J Biol Chem* **193**, 265–275.
- 939 66 Giri S & Shaha C (2019) *Leishmania donovani* parasite requires Atg8 protein for
940 infectivity and survival under stress. *Cell Death Dis* **10**, 808.
- 941 67 Dey R, Meneses C, Salotra P, Kamhawi S, Nakhasi HL & Duncan R (2010)
942 Characterization of a *Leishmania* stage-specific mitochondrial membrane protein that
943 enhances the activity of cytochrome c oxidase and its role in virulence. *Mol Microbiol*
944 **77**, 399–414.
- 945 68 Gannavaram S, Vedvyas C & Debrabant A (2008) Conservation of the pro-apoptotic

- 946 nuclease activity of endonuclease G in unicellular trypanosomatid parasites. *J Cell Sci*
947 **121**, 99–109.
- 948 69 Sahasrabuddhe AA, Bajpai VK & Gupta CM (2004) A novel form of actin in Leishmania:
949 Molecular characterisation, subcellular localisation and association with subpellicular
950 microtubules. *Mol Biochem Parasitol* **134**, 105–114.
- 951 70 Trinder P (1969) Determination of blood glucose using an oxidase-peroxidase system with
952 a non-carcinogenic chromogen. *J Clin Pathol* **22**, 158–161.
- 953 71 Hien TT, Turczyńska KM, Dahan D, Ekman M, Grossi M, Sjögren J, Nilsson J, Braun T,
954 Boettger T, Garcia-Vaz E, Stenkula K, Swärd K, Gomez MF & Albinsson S (2016)
955 Elevated glucose levels promote contractile and cytoskeletal gene expression in vascular
956 smooth muscle via rho/protein kinase C and actin polymerization. *J Biol Chem* **291**,
957 3552–3568.
- 958 72 Santara S Sen, Roy J, Mukherjee S, Bose M, Saha R & Adak S (2013) Globin-coupled
959 heme containing oxygen sensor soluble adenylate cyclase in Leishmania prevents cell
960 death during hypoxia. *Proc Natl Acad Sci U S A* **110**, 16790–16795.
- 961 73 Emanuelsson O, Brunak S, von Heijne G & Nielsen H (2007) Locating proteins in the cell
962 using TargetP, SignalP and related tools. *Nat Protoc* **2**, 953–971.
- 963 74 Krogh A, Larsson B, Von Heijne G & Sonnhammer ELL (2001) Predicting
964 transmembrane protein topology with a hidden Markov model: Application to complete
965 genomes. *J Mol Biol* **305**, 567–580.
- 966 75 Pierleoni A, Martelli PL, Fariselli P & Casadio R (2006) BaCellLo: a balanced subcellular
967 localization predictor. **22**, 408–416.
- 968 76 Neuberger G, Maurer-Stroh S, Eisenhaber B, Hartig A & Eisenhaber F (2003) Prediction
969 of peroxisomal targeting signal 1 containing proteins from amino acid sequence. *J Mol*
970 *Biol* **328**, 581–592.

Table 1. Intracellular glucose and ATP levels of untreated or zineb-treated wild type *L. major* grown in low glucose medium in absence or presence of oxaloacetate or glucose.

| Strains/Treatment ^a | Total intracellular glucose (nmol/10 ⁸ cells) ^b | Total intracellular ATP (nmol/10 ⁸ cells) ^c |
|----------------------------------|---|---|
| Untreated WT | 11.71 ± 0.62 | 56.67 ± 5.20 |
| WT + 0.625 μM Zineb | 5.96 ± 0.35** | 27.92 ± 2.59** |
| WT + 0.625 μM Zineb + 5 mM OAA | 11.31 ± 0.59 | 56.25 ± 1.52 |
| WT + 0.625 μM Zineb + 5.6 mM Glu | 11.05 ± 0.46 | 55.37 ± 2.25 |

^aWild type (WT) *L. major* promastigotes were grown in absence or presence of 0.625 μM zineb in low glucose (0.6 mM) medium for 72 h. Zineb-treated cells were either unsupplemented or supplemented with 5 mM oxaloacetate (OAA) or 5.6 mM glucose (Glu) during the 72 h duration.

^bTotal internal glucose concentration (in nmol) was experimentally determined from 2.5 x 10⁸ *L. major* cells grown in low glucose medium.

^cTotal internal ATP concentration (in nmol) was experimentally determined from 8 x 10⁶ *L. major* cells grown in low glucose medium.

± indicates SD of values from triplicate experiments.

*indicates significant difference (**p<0.01) with respect to untreated wild type strain.

Table 2. Intracellular glucose and ATP levels of wild type or mutant *L. major* strains grown in low glucose medium in absence or presence of oxaloacetate or glucose.

| Strains/Treatment ^a | Total intracellular glucose (nmol/10 ⁸ cells) ^b | Total intracellular ATP (nmol/10 ⁸ cells) ^c |
|-----------------------------------|---|---|
| WT | 11.71 ± 0.62 | 56.67 ± 5.20 |
| LmCA1 ^{+/-} | 6.80 ± 0.54** | 28.79 ± 2.96** |
| LmCA1 ^{+/-} :CM | 11.49 ± 0.55 | 57.25 ± 2.78 |
| LmCA1 ^{+/-} + 5.6 mM Glu | 12.99 ± 0.65 | 64.37 ± 2.17 |
| LmCA1 ^{+/-} + 5 mM OAA | 12.17 ± 0.58 | 57.46 ± 3.82 |
| LmCA2 ^{+/-} | 12.11 ± 0.62 | 56.06 ± 4.69 |

^aWild type (WT) or mutant *L. major* promastigotes were grown in low glucose (0.6 mM) medium for 72 hrs. During this 72 h duration, LmCA1^{+/-} strain was also grown in presence of 5 mM oxaloacetate (OAA) or 5.6 mM of glucose (Glu).

^bTotal internal glucose concentration (in nmol) was experimentally determined from 2.5 x 10⁸ *L. major* cells grown in low glucose medium.

^cTotal internal ATP concentration (in nmol) was experimentally determined from 8 x 10⁶ *L. major* cells grown in low glucose medium.

± indicates SD of values from triplicate experiments.

*indicates significant difference (**p<0.01) with respect to wild type strain.

Table 3. Intracellular glucose and ATP levels of untreated, ATR7-010-treated wild type, or mutant *L. major* strains grown in low glucose medium in absence or presence of glucose or oxaloacetate.

| Strains/Treatment ^a | Total intracellular glucose (nmol/10 ⁸ cells) ^b | Total intracellular ATP (nmol/10 ⁸ cells) ^c |
|---------------------------------|---|---|
| Untreated WT | 11.71 ± 0.62 | 56.67 ± 5.20 |
| WT + 25µM ATR7-010 | 7.17 ± 0.76** | 38.42 ± 3.79** |
| WT + 25µM ATR7-010 + 5.6 mM Glu | 12.33 ± 0.63 | 63.25 ± 4.56 |
| WT + 25µM ATR7-010 + 5 mM OAA | 13.40 ± 0.51 | 62.08 ± 4.02 |
| LmME:OE | 21.78 ± 0.53 | 98.75 ± 5.25 |

^aWild type (WT) or LmME expressing (LmME:OE) *L. major* promastigotes were grown in absence or presence of 25 µM ATR7-010 in low glucose (0.6 mM) medium for 72 h. ATR7-010-treated WT cells were either unsupplemented or supplemented with 5.6 mM glucose (Glu) or 5 mM oxaloacetate (OAA) during the 72 h duration.

^bTotal internal glucose concentration (in nmol) was experimentally determined from 2.5 x 10⁸ *L. major* cells grown in low glucose medium.

^cTotal internal ATP concentration (in nmol) was experimentally determined from 8 x 10⁶ *L. major* cells grown in low glucose medium.

± indicates SD of values from triplicate experiments.

*indicates significant difference (**p<0.01) with respect to untreated wild type strain.

Table 4. Intracellular parasite burden of glucose-starved *L. major* cells.

| Strains/Treatment ^a | Amastigotes/100 macrophages ^b | Percentage of infected macrophages ^c |
|--------------------------------|--|---|
| Untreated WT | 341.33 ± 24.84 | 91.56 ± 1.32 |
| WT + 0.625 µM Zineb | 196.33 ± 16.01** | 86.24 ± 1.19 |
| WT + 25 µM ATR7-010 | 224 ± 23** | 87.69 ± 2.29 |
| LmCA1:OE | 610.66 ± 43.52*** | 96.72 ± 2.07 |
| LmME:OE | 601 ± 41.58*** | 94.80 ± 0.53 |

^aJ774A.1 macrophages were infected with stationary-phase wild type (WT) or overexpressing (LmCA1:OE and LmME:OE) *L. major* strains grown previously in low (0.6 mM) glucose medium for 72 hrs. During the 18 hr-infection period, WT *L. major*-infected J774A.1 macrophages were treated with 0.625 µM zineb or 25 µM ATR7-010.

^bNumber of amastigotes per 100 macrophages (parasite load) for each strain/treatment was quantified by counting the total number of DAPI-stained nuclei of macrophages and amastigotes in a field. For each condition, atleast 100 macrophages (and corresponding number of amastigotes) were analysed.

^cPercentage of macrophages infected by each *L. major* strain/treatment was determined by counting total number of DAPI-stained nuclei of uninfected and infected macrophages in a field. For each condition, atleast 100 macrophages were analysed.

± indicates SD of values from triplicate experiments.

*indicates significant difference (**P<0.01, ***P<0.001) with respect to untreated WT.

Figure legends

Fig. 1. Role of CA in gluconeogenesis in mammalian cells and in *Leishmania*. (A) A schematic representation of the gluconeogenic pathway in mammalian cells showing PC-catalyzed carboxylation of pyruvate to oxaloacetate is dependent upon the HCO_3^- produced by the mitochondrial CAV enzyme. Oxaloacetate is then converted to phosphoenolpyruvate by PEPCK and thereafter gluconeogenesis proceeds through several intermediate steps. It is noteworthy that PC is absent in *Leishmania*. (B, C) Wild type *L. major* promastigotes were grown in low (0.6 mM) or high (6.2 mM) glucose medium (as indicated in the figures) in absence (0 μM ; circle) or presence of 0.156 μM (square), 0.312 μM (triangle) or 0.625 μM (inverted triangle) zineb (CA inhibitor), and growth of the cells was measured by haemocytometer-based cell counting every 24 hrs until 72 hrs of growth. Error bars represent mean \pm SD of values from 3 independent experiments. (D) Wild type (WT; circle) or LmPEPCK-overexpressing (LmPEPCK:OE; triangle) promastigotes were grown in low (0.6 mM) glucose medium in absence or presence of indicated concentrations of zineb, and growth of the cells was measured by cell counting after 72 hrs. Zineb-treated WT cells were also grown in presence of 5 mM exogenous oxaloacetate (OAA; square) in low glucose medium. For each experimental condition, cell number in untreated (0 μM zineb) samples was considered as 100%. The EC_{50} values (in μM) of zineb for WT or LmPEPCK:OE *L. major* strain grown in low glucose medium are given in the index. Error bars represent mean \pm SD of values from 3 independent experiments.

Fig. 2. Dissecting the gluconeogenic role LmCA1 and LmCA2. (A) Wild type (WT; circle), LmCA1^{+/-} (square), LmCA2^{+/-} (triangle), and LmCA1^{+/-}:CM (inverted triangle) strains were grown in low (0.6 mM) glucose medium, and their growth was monitored every 24 hrs until 72 hrs. A 36% reduction in LmCA1^{+/-} cell growth, in comparison to WT, is indicated by a black arrow. Each data point represents the mean result \pm SD from 3 independent

experiments. Asterisk indicates significant difference with respect to WT. $**P < 0.01$ (Student's t-test). (B) Wild type (WT; circle), LmCA1^{+/-} (square), and LmCA2^{+/-} (triangle) strains were grown in high (6.2 mM) glucose medium, and their growth was monitored every 24 hrs until 72 hrs. Each data point represents the mean result \pm SD from 3 independent experiments. (C) WT and LmCA1^{+/-} strains were grown in low (0.6 mM) glucose medium, in absence (black bars) or presence (grey bars) of 5 mM oxaloacetate (OAA), and the cell count was performed after 72 hrs of growth. Each data point represents the mean result \pm SD from 3 independent experiments. Asterisks indicate significant difference with respect to WT ($**P \leq 0.01$; Student's t-test) or LmCA1^{+/-} ($**P \leq 0.01$; paired t-test) strain grown in absence of OAA. (D) Wild type (WT; circle), LmCA1-overexpressing (LmCA1:OE; square) or LmCA2-overexpressing (LmCA2:OE; triangle) promastigotes were grown in low (0.6 mM) glucose medium in absence or presence of the indicated concentrations of zineb, and growth of the cells were measured by haemocytometer-based cell counting after 72 hrs of growth. Cell growth of untreated samples was considered as 100%. The EC₅₀ values (in μ M) of zineb for each *L. major* strain are given in the index. Error bars represent mean \pm SD of values from 3 independent experiments. (E) SEM images (6000 \times) of wild type (WT), LmCA1^{+/-} mutant or LmCA1^{+/-}:CM complementation *L. major* promastigotes grown in low (0.6 mM) glucose medium for 72 hrs. Scale bars: 5 μ m. (F) Representative bar graph comparing cell length (in μ m) of the wild type and mutant strains. Error bars represent average cell length \pm SD of values. Asterisks indicate significant difference with respect to WT ($***P < 0.001$) or LmCA1^{+/-} ($**P < 0.01$) strain (Student's t-test).

Fig. 3. Combined action of LmME and LmCA1 in promoting gluconeogenesis in *L. major* (A) Schematic representation of a plausible PC-independent bypass gluconeogenic pathway in *Leishmania* employing LmCA1, LmME and LmMDH. (B) 10 μ g of purified 6xHis-tagged LmME protein (63.4 kDa) was loaded on 10% SDS-PAGE, and detected by coomassie blue

staining. (C) Bar graph showing malate decarboxylation (black bar) or pyruvate carboxylation (grey bar) activity (in U/mg) in purified LmME measured spectrophotometrically. 5 μ g of purified LmME was used per assay reaction. Error bars represent mean \pm SD of values from 3 independent experiments. Asterisk indicates significant difference between malate decarboxylation and pyruvate carboxylation activity in purified enzyme. **P<0.01(Paired t-test). (D) Malate decarboxylation (circle) or pyruvate carboxylation (square) activity was measured in purified LmME in absence or presence of indicated concentrations of ATR7-010. Enzyme activity in absence of ATR7-010 (0 μ M) was considered as 100%. Error bars represent mean \pm SD of values from 3 independent experiments. The IC₅₀ values (in μ M) for ATR7-010 for malate decarboxylation or pyruvate carboxylation activity are given in the index. (E) Wild type (WT; circle), LmME-overexpressing (LmME:OE; square) or LmCA1-overexpressing (LmCA1:OE; triangle) *L. major* strains was grown in low (0.6 mM) glucose medium in absence or presence of increasing concentrations of ATR7-010, and cell number was counted microscopically at 72 hrs. During this period, ATR7-010-treated WT cells were also grown in presence of 5 mM oxaloacetate (OAA; inverted triangle) or 5.6 mM glucose (diamond). Cell number of untreated (0 μ M ATR7-010) cells was considered as 100% for each experimental set. Error bars represent mean \pm SD of values from 3 independent experiments. Respective EC₅₀ values (in μ M) are given in the index. (F) Wild type (WT; circle) or LmME-overexpressing (LmME:OE; square) strain was grown in low (0.6 mM) glucose medium in absence or presence of increasing concentrations of zineb, and cell number was counted microscopically at 72 hrs. Cell number of untreated (0 μ M zineb) cells was considered as 100% for each experimental set. Error bars represent mean \pm SD of values from 3 independent experiments. Respective EC₅₀ values (in μ M) are given in the index. (G) SEM images (6000 \times) of wild type *L. major* promastigotes grown in low (0.6 mM) glucose medium in absence (untreated) or

presence of indicated concentrations of ATR7-010. (H) Representative bar graph comparing average cell length (in μm) of promastigotes grown in absence or presence of indicated concentrations of ATR7-010. Error bars represent average cell lengths \pm SD of values from at least 50 independent measurements. Asterisks indicate significant difference with respect to untreated cells. *** $P < 0.001$, ** $P < 0.01$ (Paired t-test).

Fig. 4. Glucose-mediated regulation of LmME expression and activity. (A) Bar graph showing LmME transcript level in wild type *L. major* promastigotes, grown in high (6.2 mM) or low (0.6 mM) glucose medium for 72 hrs as determined by RTqPCR using rRNA45 as endogenous control gene and cells grown in high glucose condition as reference sample. ‘ns’ indicates insignificant difference, $P > 0.05$ (Paired t-test). (B) Protein level of LmME (63.4 kDa) in whole cell lysates of wild type (WT) *L. major* promastigotes, grown in high (6.2 mM) or low (0.6 mM) glucose medium for 72 hrs, was checked by western blotting using antibody against LmME. Expression of β -actin (42 kDa), detected by anti- β -actin antibody was considered as the loading control. (C) Bar graph comparing relative LmME band intensity of wild type (WT) strain grown in high or low glucose medium from triplicate experiments. Error bars represent mean \pm SD of values from 3 independent experiments. Asterisk indicates significant difference with respect to WT cells grown in high glucose medium. ** $P < 0.01$ (Paired t-test). (D) Wild type (WT) *L. major* promastigotes, grown in high (6.2 mM) or low (0.6 mM) glucose medium for 48 hrs, were immunostained with an antibody against LmME (green), and visualised with a Zeiss LSM 710 confocal microscope using appropriate filter sets. DAPI (blue) was used to stain the nucleus. Scale bars: 5 μm . (E) Representative bar graph comparing mean LmME fluorescence intensity (in arbitrary units; AU) of wild type (WT) strain grown in high or low glucose medium. At least 50 *L. major* cells were analyzed per experimental condition. Error bars represent mean \pm SD of values from 3 independent experiments. Asterisk indicates significant difference in mean

fluorescence intensity between WT cells grown in high and low glucose condition. $**P < 0.01$ (Paired t-test). (F) Malate decarboxylation (black bars) or pyruvate carboxylation (grey bars) activity (in U/mg) was spectrophotometrically measured in whole cell lysate of wild type *L. major* promastigotes grown in high (6.2 mM) or low (0.6 mM) glucose medium for 72 hrs. 100 μ g of whole cell lysate was used per assay reaction. Error bars represent mean \pm SD of values from 3 independent experiments. Asterisk indicates significant difference between malate decarboxylation and pyruvate carboxylation activity, or between pyruvate carboxylation activity in whole cell lysates of wild type *L. major* promastigotes grown in high or low glucose medium. $**P < 0.01$, $***P < 0.001$ (Paired t-test).

Fig. 5. Subcellular localization of LmME. (A) *L. major* cells stably expressing LmME as a C-terminal GFP-tagged protein (LmME-GFP) were stained with MitoTrackerRed CMXRos (red). The pattern of LmME and MitoTracker Red colocalisation (merge) was visualised with a Zeiss LSM 710 confocal microscope using appropriate filter sets. DAPI (blue) was used to stain the nucleus. These are representative images from multiple experiments. Scale bars: 2 μ m. (B) Wild type *L. major* cells were subjected to fractionation into cytoplasmic and mitochondrial fractions. Distribution of LmME (63.4 kDa) in the cell fractions was determined by western blotting with an antibody against LmME. Authenticity of the cell fractions was verified by western blotting using antibodies LmCA1 (as cytosolic marker, 35.4 kDa) and LmAPX (as mitochondrial marker, 30 kDa). Shown are representative blots from at least 3 independent experiments.

Fig. 6. An illustrative model of the initial steps of gluconeogenesis in *Leishmania* highlighting the functional partnership between LmCA1 and LmME. *Leishmania* parasites proliferate in the amino acid-rich phagolysosomal environment of the host macrophages where glucose availability is scarce. Gluconeogenic amino acids, taken up by the parasite from its surroundings, are metabolized to pyruvate in the cytosol. Pyruvate can be transported

to the mitochondria through pyruvate carrier protein. Mitochondrial LmME, by virtue of its pyruvate carboxylase activity, can convert pyruvate to malate. The cytosolic LmCA1 can facilitate this carboxylation reaction by producing the crucial CO₂, which can easily diffuse into the mitochondria. Malate eventually gets transported to the glycosome via putative malate transporters, where it is then converted to oxaloacetate by gMDH. Further downstream pathways of gluconeogenesis shown in the figure are self-explanatory. Abbreviations used: LmCA1; *L. major* carbonic anhydrase 1, LmME; *L. major* malic enzyme, gMDH; glycosomal malate dehydrogenase, PEPCK; Phosphoenolpyruvate carboxykinase, PEP; Phosphoenolpyruvate, F6-P; Fructose 6-phosphate, G6-P; Glucose 6-phosphate, PP shunt; Pentose Phosphate shunt. The image was created using the software, BioRender.com.

Figure 1

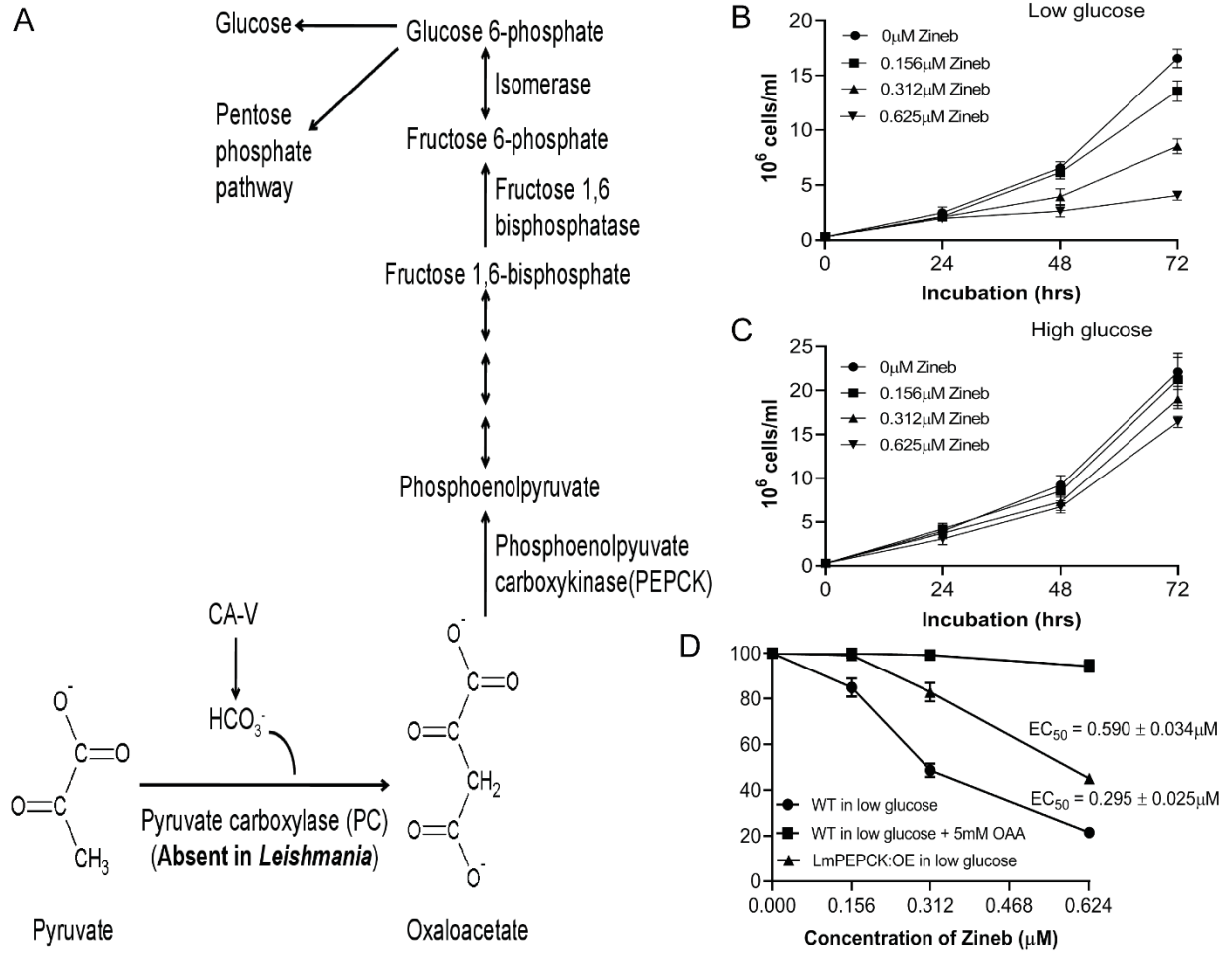


Figure 2

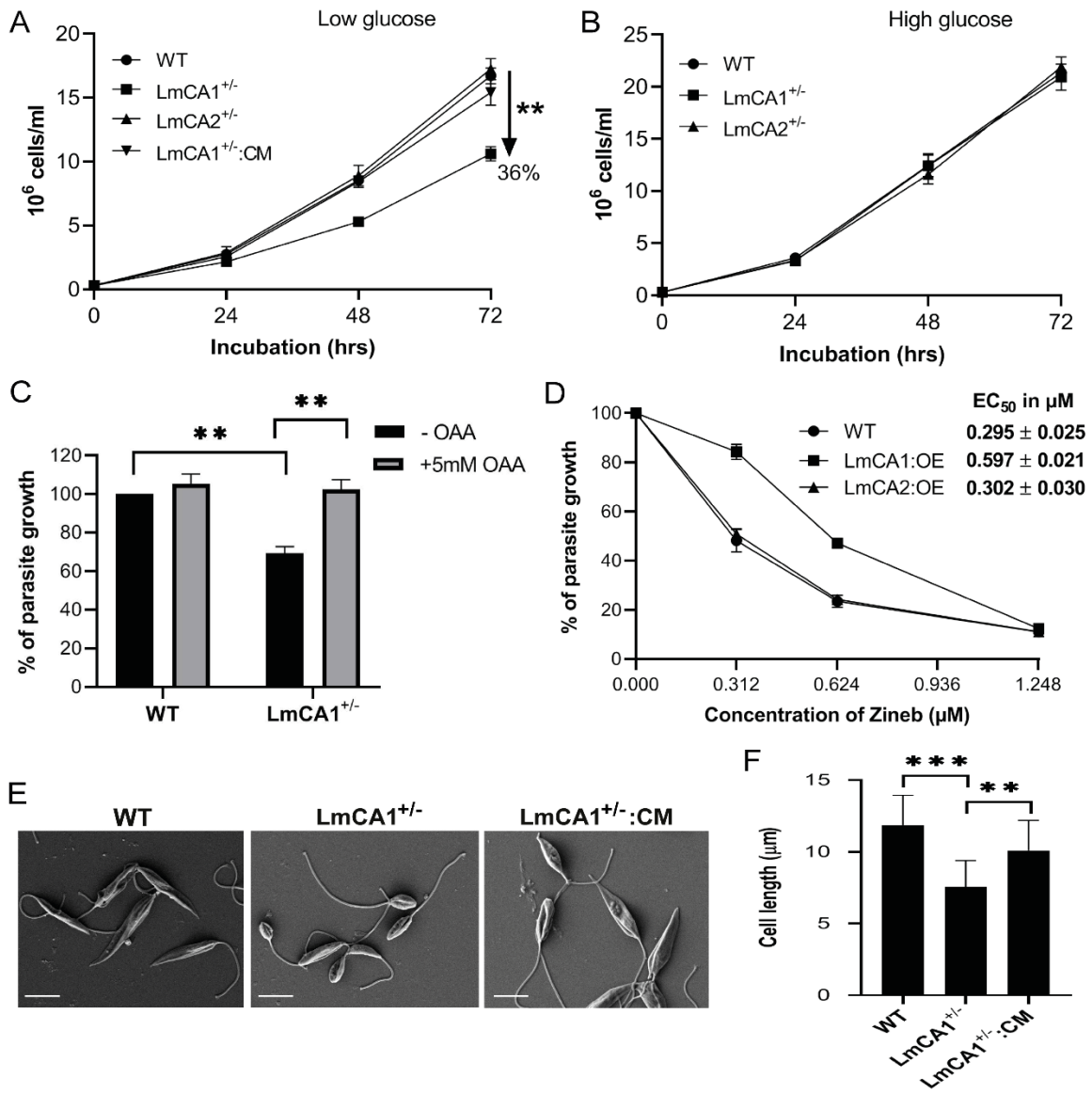


Figure 3

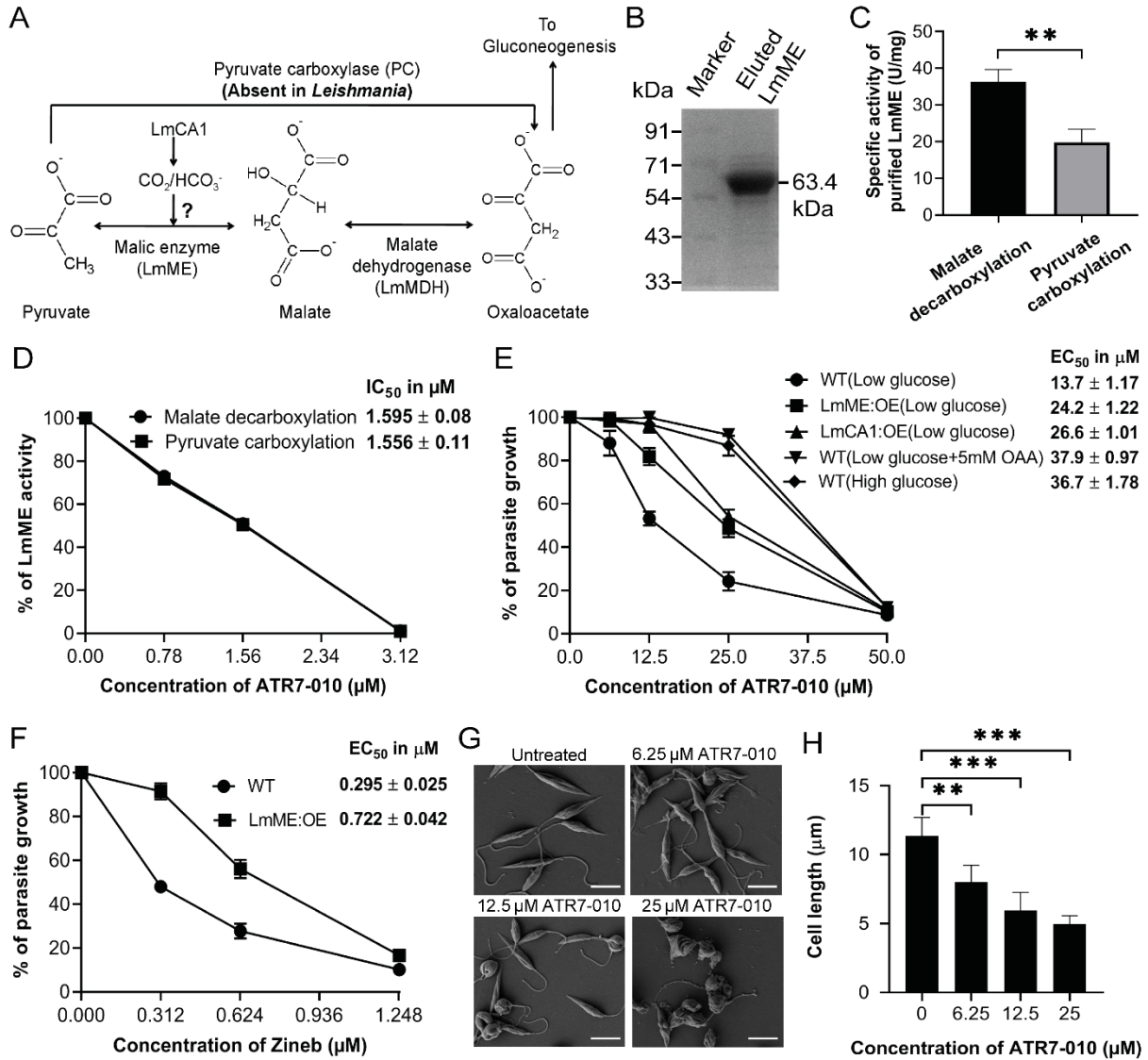


Figure 5

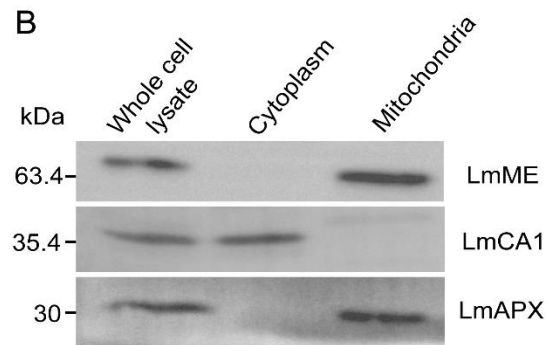
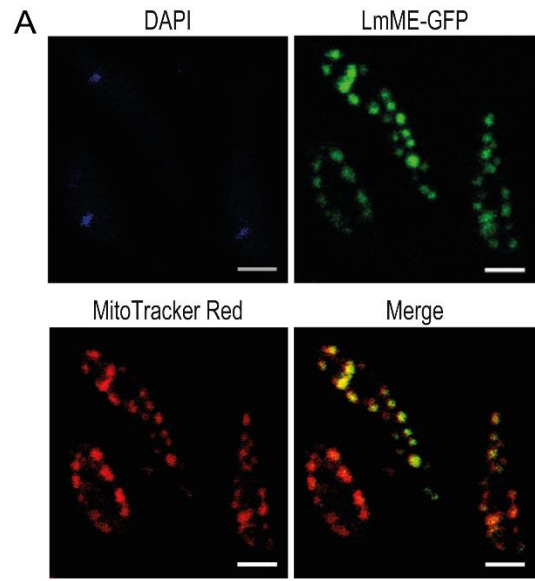
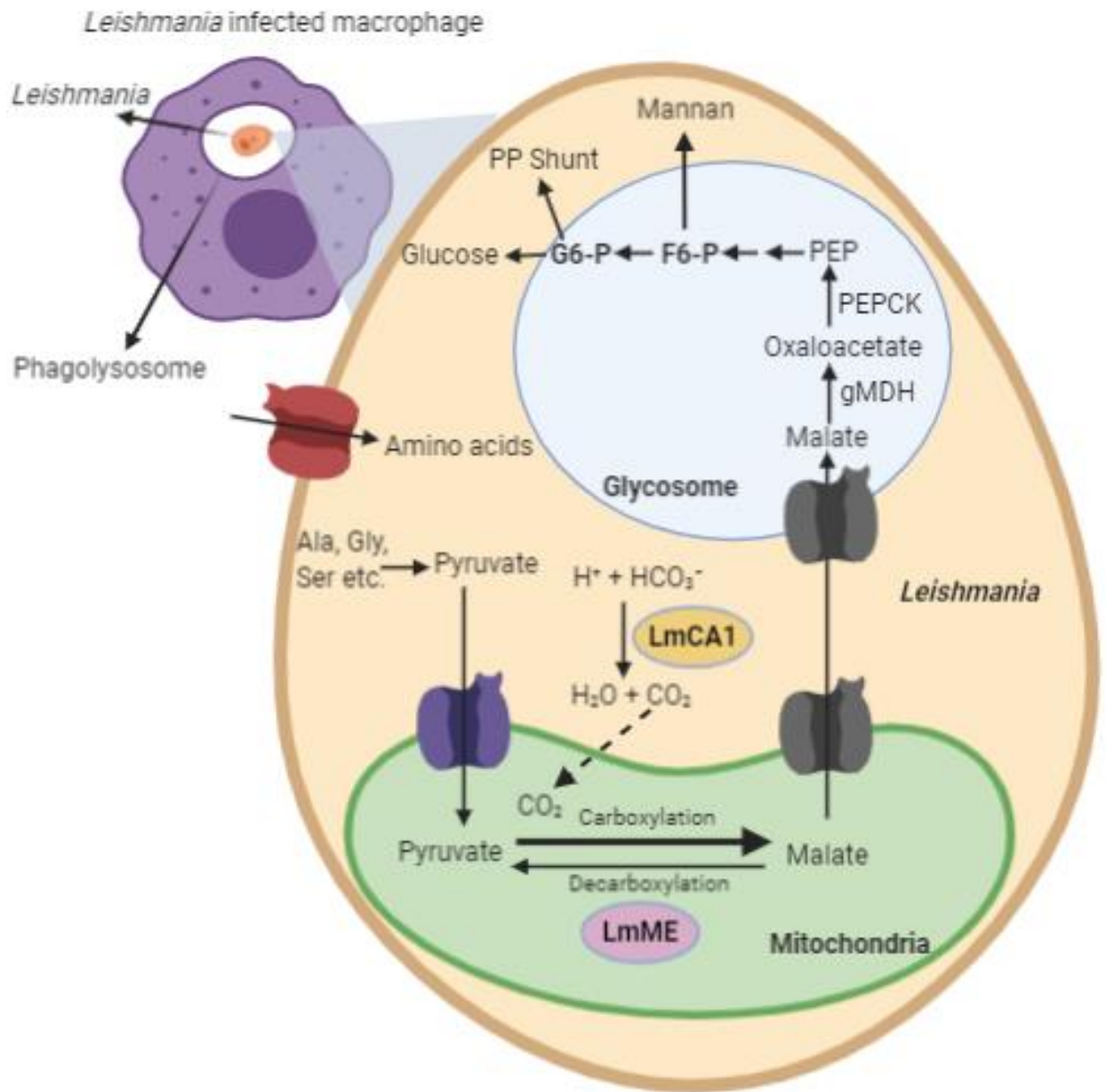


Figure 6



Supplementary materials

Table S1. Software-based prediction of subcellular localization of LmME.

| Protein of interest | Software ^a | Analysis report | Inference |
|---------------------|-----------------------|---|---|
| LmME | TargetP v1.1 | Mitochondrial signal peptide is present | Since LmME possesses a mitochondrial signal peptide sequence and has no transmembrane domain, it was predicted to be a mitochondrial matrix protein |
| | TMHMM v2.0 | Transmembrane domain is absent | |
| | BaCelLo | Nuclear localization signal is absent | |
| | PTS1 Predictor | Peroxisome targeting signal 1 is absent | |

^aSubcellular localization for LmME was predicted by analyzing its primary sequence using online prediction software such as, TargetP v1.1 to predict presence of any of the N-terminal signal sequence for targeting a protein to ER, mitochondria or chloroplast, TMHMM v2.0 to predict transmembrane helices, BaCelLo to predict presence of a nuclear localization signal, and PTS1 predictor to predict peroxisome targeting signal 1.

Table S2. Primers used in this study.

| Primer | Primer sequence (5'-3') ^a | Purpose |
|--------|--|---|
| P1 | GCGCGGATCC ACCATGGCCCCGATCATCCACC | Cloning of OE construct & semi-quantitative RT-PCR of LmPEPCK |
| P2 | GCGCGATATCCTACAGATGAGCCGTCTCCACGTA | |
| P3 | GCGCCCCGGGATGTCGCTGTGCAGCTGC | Cloning of OE construct & semi-quantitative RT-PCR of LmCA1 |
| P4 | GCGCCCCGGGCTACAGCTGCCCGTAGCGC | |
| P5 | GCGCGGATCCATGAAGACACTTCCTTTCTGTGCCAC | Cloning of OE construct & semi-quantitative RT-PCR of LmCA2 |
| P6 | GCGCGGATCCTTACCGCACAGCCACGGTAC | |
| P7 | GCGCGGATCCACCATGTTTGCCAAGTCGCTGGTGC | Cloning of GFP construct of LmME |
| P8 | GCGCGATATCGGAATCAACTCCTTCTCCAGGTAGTAGT | |
| P9 | GCGCGAATTCTTTGCCAAGTCGCTGGTGCATC | Cloning of LmME bacterial expression construct & semi-quantitative RT-PCR |
| P10 | GCGCAAGCTTTTAGCGAATCAACTCCTTCTCCAGGTAGTAGT | |
| P11 | GCGCGAATTCTCGCTGTGCAGCTGC | Cloning of LmCA1 bacterial expression construct |
| P12 | GCGCGAATTCCTACAGCTGCCCGTAGC | |
| P13 | CCTACCATGCCGTGTCCTTCTA | Semi-quantitative RT-PCR & Real-time PCR of rRNA45 |
| P14 | AACGACCCCTGCAGCAATAC | |
| P15 | ATGTTTGCCAAGTCGCTGGTGC | Real-time PCR of LmME |
| P16 | CGTTCATGTGCGACCGCTCT | |
| P17 | ATCGTGCAGCTGAACCCGG | Real-time PCR of LmCA1 |
| P18 | CGATTGCGTACTGGATAACAGCG | |
| P19 | GCGCGGATCCACCATGTTTGCCAAGTCGCTGGTGC | Cloning of OE construct of LmME |
| P20 | GCGCGATATCTTAGCGAATCAACTCCTTCTCCAGGTAGTAGT | |

^aRestriction sites in primer sequences are highlighted in bold.

Legends for supplementary figures

Figure S1. Verification of *L. major* strains overexpressing different genes. Measurement of transcript abundance of LmPEPCK (1578 bp), LmCA1 (921 bp), LmCA2 (1887 bp), or LmME (1722 bp) in wild type (WT) or overexpressing (OE) *L. major* strains by semi-quantitative RT-PCR using primers listed in Table S2 (represented by lanes marked as '+'). Respective negative control reactions without RT enzyme are represented by lanes marked as '-'. rRNA45 gene (143 bp) was used as the endogenous control.

Figure S2. Chemical structures of ME inhibitors used in this study, ATR4-003, ATR6-001, and ATR7-010.

Figure S3. Cloning and expression of 6xHis-tagged LmME in bacterial expression system. (A) Verification of LmME/pET28a+ clone upon restriction digestion with EcoRI and HindIII showing two expected fragments for vector backbone (5369bp) and LmME (1722 bp). (B) Coomassie blue-stained SDS-PAGE showing LmME (63.4 kDa) expression in BL21(DE3) *E. coli* cells grown in presence of 0.5mM IPTG (+IPTG) for 8 hrs at 20°C. LmME was not expressed in bacterial cells grown in absence of IPTG (-IPTG).

Figure S4. Characterization of LmME or LmCA1 antibodies. (A) 0.5 µg purified LmME protein or 80 µg wild type *L. major* whole cell lysate was subjected to SDS-PAGE and immunostained with anti-LmME antibody (1:4000). LmME band was detected at its predicted molecular weight (63.4 kDa) (B) 9.25 µg purified LmCA1 protein or 120 µg wild type *L. major* whole cell lysate was subjected to SDS-PAGE and immunostained with anti-LmCA1 antibody (1:1000). LmCA1 band was detected at its predicted molecular weight (35.4 kDa).

Figure S5. Constitutive expression of LmCA1 in *L. major* cells. (A) Bar graph showing LmCA1 transcript levels in wild type *L. major* promastigotes, grown in high (6.2 mM) or low (0.6 mM) glucose medium for 72 hrs determined by RTqPCR using rRNA45 as endogenous

control gene and cells grown in high glucose condition as reference sample. (B) Protein level of LmCA1 (35.4 kDa) in whole cell lysates of wild type (WT) *L. major* promastigotes, grown in high (6.2 mM) or low (0.6 mM) glucose medium for 72 hrs, was checked by western blotting using antibody against LmCA1. Expression of β -actin (42 kDa), detected by anti- β -actin antibody was considered as loading control.

Figure S6. Verification of LmME-GFP clone. Restriction digestion of the LmME-GFP construct with BamHI and EcoRV showing two expected fragments for pXG-GFP vector backbone (7570bp) and LmME without a stop codon (1719 bp).

Figure S7. Effect of ATR7-010 treatment on proliferation of J774A.1 macrophage cells. J774A.1 macrophages were grown in absence or presence of indicated concentrations of ATR7-010 and cell growth was measured microscopically after 72 hrs. The EC_{50} value (in μ M) of ATR7-010 for J774A.1 cells is given in the index. Error bars represent mean \pm SD of values from 3 independent experiments.

Figure S1

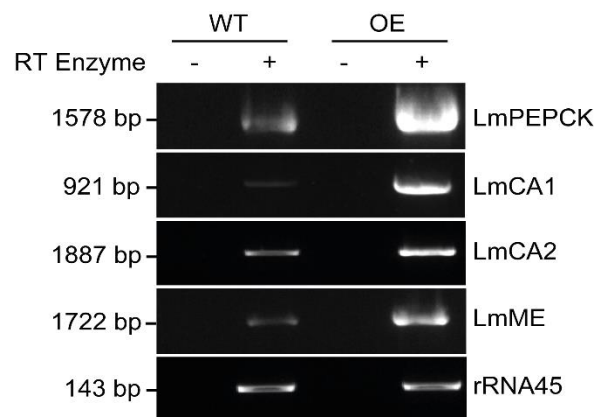


Figure S2

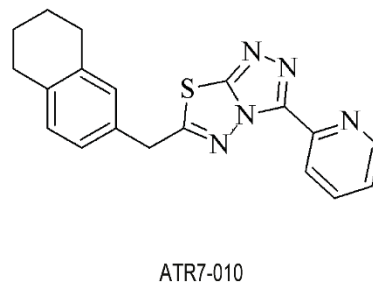
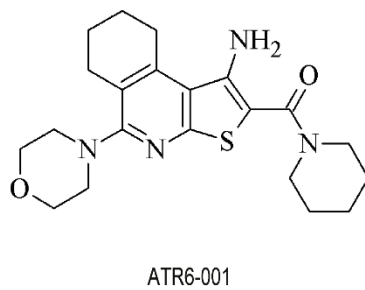
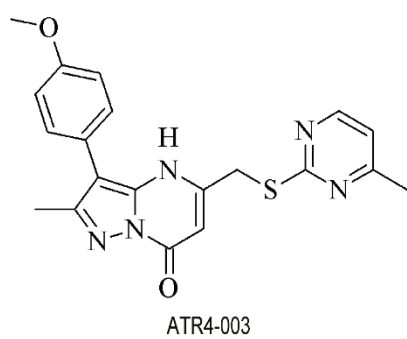


Figure S3

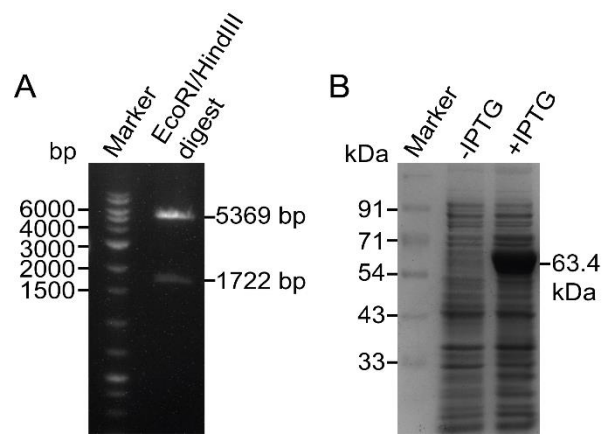


Figure S4

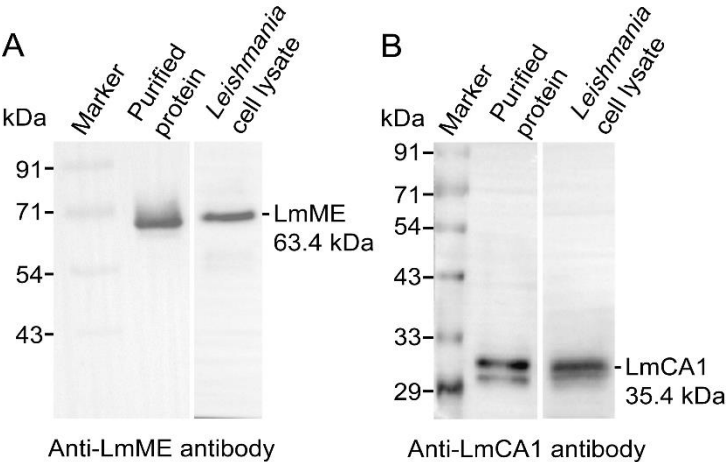


Figure S5

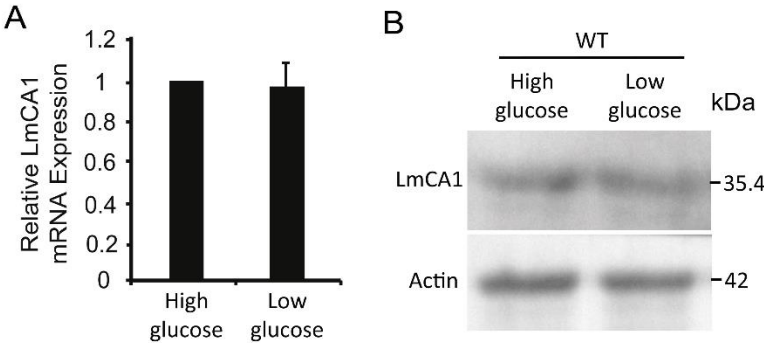


Figure S6

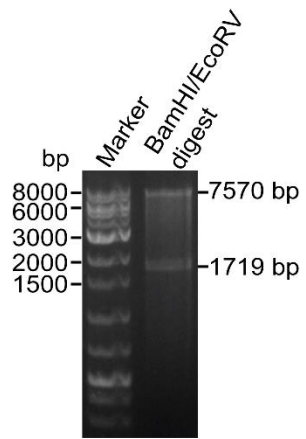


Figure S7

